

Bio-orthogonally double cross-linked alginate-gelatin hydrogels with tunable viscoelasticity for cardiac tissue engineering

Original

Bio-orthogonally double cross-linked alginate-gelatin hydrogels with tunable viscoelasticity for cardiac tissue engineering / Testore, D., Zoso, A., Paoletti, C., Groppo, S., Marcello, E., Chiono, V.. - In: MATERIALS TODAY BIO. - ISSN 2590-0064. - 34:(2025). [10.1016/j.mtbio.2025.102121]

Availability:

This version is available at: 11583/3002267 since: 2025-07-31T08:38:03Z

Publisher:

Elsevier

Published

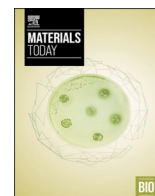
DOI:10.1016/j.mtbio.2025.102121

Terms of use:

This article is made available under terms and conditions as specified in the corresponding bibliographic description in the repository

Publisher copyright

(Article begins on next page)



Bio-orthogonally double cross-linked alginate-gelatin hydrogels with tunable viscoelasticity for cardiac tissue engineering

Daniele Testore^{a,b,*}, Alice Zoso^{a,b}, Camilla Paoletti^{a,b}, Sara Groppo^c, Elena Marcello^{a,b}, Valeria Chiono^{a,b,**}

^a Department of Mechanical and Aerospace Engineering, Politecnico di Torino, Turin, Italy

^b POLITO BiomedLab, Politecnico di Torino, Torino, Italy

^c Department of Control and Computer Engineering, Politecnico di Torino, Turin, Italy

ARTICLE INFO

Keywords:

Hydrogels
Click chemistry
Bio-orthogonal
Viscoelasticity
Cardiac tissue engineering

ABSTRACT

Growing evidence has shown that cells respond to the viscoelastic properties of the extracellular matrix (ECM), particularly its stress-relaxation, which influences their spreading, proliferation, and remodeling. Since cardiac tissue viscoelasticity plays a key role in modulating cellular mechanosensing, the development of biomimetic viscoelastic hydrogels is highly needed in cardiac tissue engineering (CTE). This work presents bio-orthogonal double cross-linked alginate-gelatin hydrogels with tunable viscoelasticity, designed to replicate the dynamic mechanical properties of cardiac ECM. Alginate and gelatin were functionalized with azide groups and cross-linked by a 4-arm-dibenzocyclooctyne (DBCO) crosslinker using strain-promoted azide-alkyne cycloaddition (SPAAC) with 0.5:1 (AG_Click(R0.5)) and 1:1 (AG_Click(R1)) DBCO:azide molar ratios. Calcium ions were also introduced to obtain double cross-linked hydrogels (AG_DC(R0.5) and AG_DC(R1)). Rheology showed that hydrogels exhibited tunable stiffness and stress relaxation, closely mimicking the properties of native cardiac tissue. The behavior of human cardiac fibroblasts (HCFs), seeded on hydrogels, was analyzed. When compared to purely elastic polyacrylamide (pAAm) hydrogels with comparable stiffness, soft stress-relaxing hydrogels (AG_Click(R0.5) and AG_DC(R0.5)) were found to promote cell spreading area, while stiffer stress-relaxing hydrogels (AG_Click(R1) and AG_DC(R1)) enhanced asymmetric cell elongation, reflecting substrate-mediated mechanosensing. Additionally, HCFs showed high viability when cultured in 3D hydrogels over 7 days. Overall, rapid gelation, biocompatibility, and tunable viscoelastic properties of bio-orthogonal double cross-linked alginate-gelatin hydrogels support their use as injectable formulations or engineered cardiac tissues for CTE.

1. Introduction

Myocardial infarction (MI) results from coronary artery occlusion, leading to cardiomyocyte death and the formation of fibrous scar tissue, which impairs heart function and may lead to heart failure [1,2]. Currently available treatments focus on symptom management, and are unable to address cardiomyocyte loss and to regenerate the damaged tissue [3]. Cardiac tissue engineering (CTE) strategies based on biomimetic hydrogels have been proposed to provide structural support and bioactive cues for cardioprotection and tissue regeneration [4]. However, one main challenge in CTE is the design of hydrogels able to replicate the complex mechanical properties of cardiac extracellular matrix (ECM), characterized by nonlinear viscoelasticity and anisotropic

behavior [5–7]. Particularly, a growing body of evidence has demonstrated that cells sense and respond to the viscoelastic features of ECMs, challenging the traditional stiffness-centric interpretation of mechano-transduction [8]. The viscoelastic properties of hydrogels, particularly their stress-relaxation ability, are now recognized as key factors in supporting the mechanotransduction pathways that influence cell behavior, migration, and ECM remodeling [9–11]. Recent strategies for modulating the viscoelasticity of hydrogels involved reversible cross-links that can rapidly dissociate and reform, such as ionic interactions [11] and chemical crosslinks based on Diels-Alder reaction [12], imine chemistry [13], Schiff-base reaction [14], reversible boronated esterification [15], thiol-thioester exchange [16], hydrazone and oxime formation [17,18]. Moreover, several reports have investigated

* Corresponding author. Department of Mechanical and Aerospace Engineering, Politecnico di Torino, Turin, Italy.

** Corresponding author. Department of Mechanical and Aerospace Engineering, Politecnico di Torino, Turin, Italy.

E-mail addresses: daniele.testore@polito.it (D. Testore), valeria.chiono@polito.it (V. Chiono).

the design of double-crosslinked hydrogel networks with tunable stiffness and viscoelasticity through the combination of reversible physical and permanent chemical cross-links [12,18,19]. In both 2D and 3D cultures, the tuning of hydrogel viscoelasticity showed a significant impact on its time-dependent mechanical properties which, in turn, regulate the spreading, migration, and proliferation of various cell types, such as myoblasts, fibroblasts, pre-osteoblasts and cancer cells [10,11, 20–23]. Moreover, viscoelastic hydrogels were also found to support lineage-specific differentiation of stem cells and ECM deposition, thereby affecting tissue regeneration [11]. Despite this evidence, studies addressing the effect of viscoelastic hydrogels on cardiac cell behavior are still missing. Most efforts have been focused on studying the stiffness-dependent behavior of cardiac cells and on the development of mechanically robust cardiac patches able to withstand the mechanical forces of the heart [6,24–26]. However, these approaches have been limited by the use of multi-step harsh and cytotoxic cross-linking processes [6]. Bio-orthogonal click chemistries, including strain-promoted azide-alkyne cycloaddition (SPAAC), have emerged as rapid, catalyst-free, specific, and biocompatible cross-linking techniques, with no cytotoxic by-products, making them ideal as injectable hydrogels and 3D cell encapsulation systems for both *in vitro* and *in vivo* applications [27–31]. Furthermore, the combination of bio-orthogonal covalent and physical cross-linking into a double-cross-linked network might allow fine modulation of hydrogel viscoelasticity [12,18,19].

This work was aimed at the development of novel biomimetic bio-orthogonal double cross-linked alginate-gelatin hydrogels with tunable viscoelastic properties for cardiac tissue engineering applications. Alginate is a natural polysaccharide with highly tunable properties, cost-effectiveness non-immunogenicity, and non-toxicity, but also bio-inert [32]. On the other hand, gelatin is a protein derived from collagen that has cell-responsive properties that make it favorable to design biomimetic substrates in CTE applications [33]. Alginate and gelatin were modified to expose lateral azide functionalities and, then, hydrogels were formed by bio-orthogonal SPAAC reaction of the polymers with dibenzocyclooctyne (DBCO) 4-arm crosslinker. Double-crosslinked hydrogels were formed by additional ionic cross-linking of alginate chains through calcium ions. Different DBCO:azide molar ratios were tested to tune the viscoelastic properties of the double-crosslinked hydrogels. The hydrogels were thoroughly characterized for their physicochemical properties, particularly focusing on their rheological behavior. *In vitro* cytocompatibility, adhesion and spreading tests were also performed using human cardiac fibroblasts (HCFs) seeded on hydrogels. Additionally, the viability of HCFs 3D encapsulated within hydrogels, was evaluated. To the best of our knowledge, this is the first study investigating the impact of stress-relaxing substrates on cardiac cells mechanosensing, thus providing early evidence on the potential impact of double crosslinked alginate-gelatin hydrogels for CTE.

2. Materials and methods

2.1. Materials

Gelatin from cold water fish skin, phosphate buffered saline (PBS, pH 7.4), tris(hydroxymethyl)aminomethane (TRIS), dimethyl sulfoxide (DMSO) and sodium chloride (NaCl) were purchased from Sigma-Aldrich (Milano, Italy). 2-(N-morpholino)ethane sulfonic acid (MES) was purchased from TCI Chemicals. Medium viscosity alginic acid sodium salt extracted from *macrocytys pirifera* algae was purchased from MP Biomedicals (Irvine, United States of America). Linear azido-(polyethylene glycol)₃-amine (azido-PEG3-amine) and dibenzocyclooctyne-(polyethylene glycol)₄-amine (DBCO-PEG4-amine) were purchased from Click Chemistry Tools (Scottsdale, United States of America). 4-arm-(polyethylene glycol)-dibenzocyclooctyne (4-arm-PEG-DBCO, $M_n = 5000$ Da) was purchased from Creative PEGworks (Chapel Hill, USA). 1-(3-Dimethylaminopropyl)-3-ethylcarbodiimide hydrochloride (EDC), N-Hydroxysuccinimide (NHS) and calcium chloride ($CaCl_2$) were

purchased from Fisher Scientific (Milano, Italy). Deionized water (dH_2O) was obtained by means of a reverse osmosis purification equipment.

2.2. Alginate and gelatin molecular weight measurements

The viscosity-averaged molecular weight (M_{η}) of both alginate and gelatin was determined by measuring their intrinsic viscosity with an Ubbelohde capillary viscometer [34–39] (see Supplementary Informations for further details).

2.3. Alginate functionalization with azide groups

The conjugation of azido-PEG3-amine molecules to carboxyl groups (COOH) on alginate strands was carried out through EDC/NHS coupling chemistry according to the protocol reported by Moody C. et al. [40]. Herein, the moles of employed reagents were related to the moles of carboxyl groups on alginate (mol_{COOH}), considering its repeating unit. Alginic acid sodium salt was dissolved in MES buffer (0.1M MES, 0.3M NaCl, pH: 6.5 adjusted by 1M NaOH addition) overnight at a final concentration of 0.5 % w/v. Following this, azido-PEG3-amine (1 mol/ mol_{COOH}) was added to the solution and the mixture was stirred for an additional hour at room temperature. Then, a combination of EDC (4 mol/ mol_{COOH}) and NHS (2 mol/ mol_{COOH}) was added to the stirring mixture in three separate equal portions, with each dose being added 8 h apart, and the solution was stirred for additional 8 h. Finally, dialysis was performed using membranes with a weight average molecular weight (M_w) cutoff of 6–8 kDa (SpectraPor, Spectrum Labs, Greece) against 3 L of dH_2O with progressively decreasing NaCl content at each exchange (performed twice a day) for overall 3 days. The dialyzed solution was frozen at $-20^\circ C$, subsequently freeze-dried for 5 days using a CoolSafe 4–15L freeze-dryer (Labogene, Scandinavia). The lyophilized alginate-azide (ALG-Az) powder was kept under vacuum until use.

2.4. Gelatin functionalization with azide groups

Covalent grafting of azido-PEG3-amine molecules to carboxyl groups on gelatin strands was also performed by EDC/NHS coupling chemistry. Herein, the moles of employed reagents were related to the moles of carboxyl groups (mol_{COOH}) on gelatin from cold water fish skin, based on its average content of peptides with lateral carboxyl groups (i.e., aspartic acid and glutamic acid) [41]. Different quantities and combinations of reagents (Supplementary Table S1) were investigated to enhance coupling efficiency. Gelatin was dissolved in MES buffer (0.1M MES, pH: 6.1 adjusted by 1M NaOH addition) for 30 min at room temperature, reaching a final concentration of 1 % w/v. Subsequently, azido-PEG3-amine was added to the solution, and the mixture was stirred for an additional hour at room temperature. Following this, a combination of EDC and NHS was introduced within the stirring reaction mixture in three separate equal portions, with each portion added at 8-h intervals. Afterwards, the solution was stirred for additional 8 h. Finally, the solution underwent dialysis through membranes with M_w cutoff of 3.5 kDa (SpectraPor, Spectrum Labs, Greece), against 3 L of dH_2O for 3 days, with the solution being changed 2 times per day. Dialyzed solution was frozen at $-20^\circ C$ and freeze-dried for 5 days. The lyophilized gelatin-azide (GEL-Az) powder was kept under vacuum until its use.

2.5. Fourier transform infrared spectroscopy

The conjugation of azide groups on alginate and gelatin chains was analyzed by attenuated total reflectance-infrared spectroscopy (ATR-FTIR). The analysis was carried out on lyophilized samples obtained from the functionalization reactions. Spectra were recorded on a Thermo Scientific Nicolet iS50 FTIR Spectrometer (Milano, Italy) equipped with a diamond crystal ATR accessory. For each sample, ATR

spectra were collected in the 4000–450 cm^{-1} wavenumber range with a resolution of 4 cm^{-1} . Spectra of unmodified alginate and gelatin powders were also taken as reference.

2.6. Quantification of azides on alginate and gelatin

The quantification of azide groups on both alginate-azide and gelatin-azide was conducted by UV–Vis spectroscopy, adapting from a previously reported protocol (see Supp. Info. for details) [40].

2.7. Hydrogels preparation

ALG-Az, GEL-Az and 4-arm-PEG-DBCO were dissolved in PBS respectively at 8 % w/v, 32 % w/v and 6 % w/v concentrations and gently stirred at room temperature until homogeneous stock solutions were obtained. Bio-orthogonally chemically cross-linked Alginate-Gelatin hydrogels (AG_Click) with 8 % w/v overall alginate/gelatin (20/80 wt/wt.) concentration and different cross-linking rates (listed in Table 1), were prepared as follows: specific volumes of ALG-Az and GEL-Az stock solutions were loaded in two separate 1 mL Luer lock syringes. The two syringes were connected through a female-female Luer lock connector and the solutions were gently mixed until homogeneous, while avoiding to introduce air bubbles into mixture. Similarly, a diluting volume of PBS was added to the mixture. Finally, 4-arm-PEG-DBCO stock solution was thoroughly and quickly mixed to the ALG-Az and GEL-Az mixture at different azide:DBCO molar ratios (R). Hydrogel samples were prepared by casting 100 μL of the solution into cylindrical homemade silicone molds (1 mm diameter, 1 mm thickness) and allowing the strain-promoted azide-alkyne cycloaddition (SPAAC) to proceed for at least 30 min at room temperature. The effective SPAAC cross-linking degree was verified by quantifying unreacted azides within formed hydrogels through UV–Vis spectroscopy, as described in the previous paragraph (see Supp. Info. for details). To obtain double cross-linked hydrogels (AG_DC), AG_Click hydrogel disks were formed and then each sample was incubated in 300 μL of 0.1 M CaCl_2 solution. After 30 min CaCl_2 was removed and the samples were washed three times with PBS.

2.8. Rheological analysis

Rheological testing was performed to investigate SPAAC cross-linking kinetics of AG_Click hydrogels and to determine viscoelastic properties of AG_Click and AG_DC hydrogels. All rheological experiments were performed on an Anton PAAR Modular Compact Rheometer (Physica MCR 302, Graz, Austria) in parallel-plate mode (25 mm diameter, 0.2 mm of gap for time sweep measurements and 15 mm diameter, 0.5 mm of gap for further testing) at 37 °C, and a solvent trap filled with dH_2O was exploited to reduce sample evaporation. To determine gelation kinetics, 150 μL of AG_Click precursor solution was prepared as described in section 2.9 and immediately dispersed between the parallel plates. Time sweep measurements were carried out at constant 1 % shear strain and 1 Hz angular frequency. The evolution of the storage modulus (G') as a function of time was recorded to determine the cross-linking kinetics. Specifically, sol-gel phase transition was evaluated by recording the cross-over points (i.e., the time at which $G''/G' =$

Table 1

Compositions of the different bio-orthogonal Alginate-Gelatin hydrogels, with corresponding sample codes.

Sample Code	ALG-Az (% w/v)	GEL-Az (% w/v)	DBCO:Azide (mol: mol)	Ca^{2+} (\pm)
AG_Click (R0.5)	1.6	6.4	0.5:1	–
AG_Click(R1)	1.6	6.4	1:1	–
AG_DC(R0.5)	1.6	6.4	0.5:1	+
AG_DC(R1)	1.6	6.4	1:1	+

$\tan \delta = 1)$.

Viscoelastic properties (i.e., G' , storage modulus; G'' , loss modulus and $\tan \delta$, loss tangent) of formed hydrogel disks (fully gelled and equilibrated in PBS) were evaluated through oscillatory frequency sweep measurements (frequency varying from 0.1 to 100 rad/s) at a strain amplitude of 1 %, in the linear viscoelastic region (LVR) of samples. Young's modulus (E) at 1 Hz was calculated as previously reported [42]:

$$E = 2\sqrt{G'^2 + G''^2} * (1 + \nu)$$

where G' is the storage modulus, G'' is the loss modulus, and ν is Poisson's ratio. The Poisson's ratio of the hydrogels was assumed to be 0.5.

Shear stress relaxation measurements were carried out using a previously published method [18]. In detail, a constant strain of 10 % was applied to hydrogel samples and kept constant along the test. The rates of shear stress relaxation were evaluated by recording the time taken by the samples to relax the shear stress to half of its initial value (i.e. relaxation time: $\tau_{1/2}$). As a purely elastic control, polyacrylamide hydrogels (described in the Supplementary Table S2) were prepared following a previously reported and well-known method. Frequency sweeps and stress relaxation measurements of polyacrylamide hydrogels were also performed using the same procedure described for AG_Click and AG_DC hydrogels. All rheological tests were conducted in triplicate.

2.9. In vitro swelling and degradation behavior

The swelling and degradation behavior of hydrogels was evaluated by a gravimetric method. The initial weight (W_i) of hydrogels was measured. Subsequently, samples (100 μL) were incubated in 500 μL of PBS solution w/o collagenase type II as degradation enzyme (2.5 U/mL, Worthington Biochemical Corporation, USA), per hydrogel at 37 °C. The buffer was refreshed every three days. At designated time points, the buffer solution was removed from Eppendorf tubes containing the hydrogel samples, which were subsequently weighed (W_t). Fresh buffer was then replenished. The swelling and degradation percentage of hydrogels was assessed using the following equation:

$$\text{Swelling / Degradation \%} = \frac{W_t - W_i}{W_i} * 100$$

where, positive values were considered as swelling (%) and negative values were considered as degradation (w%). Three parallel samples for each tested formulation were analyzed.

2.10. Gelatin release

Release of unreacted gelatin from cross-linked hydrogels was evaluated by a colorimetric test. Briefly, formed AG_Click and AG_DC samples (100 μL) were weighed and then each sample was immersed in 500 μL of PBS at 37 °C up to 14 days. At predetermined time points (1, 3, 7 and 14 days), the solution was collected for gelatin release evaluation and fresh PBS was added to the samples. Gelatin concentration was determined by the BCA protein assay [43], through a calibration curve obtained from solutions at known gelatin concentrations. The absorbance of each solution at 562 nm was measured by an UV–Vis spectrophotometer (Varioskan™ LUX, Thermo Scientific, United States). The released gelatin fraction was calculated as follows:

$$\text{Gelatin Release \%} = \frac{[\text{Gelatin}]_{\text{supernatant}}}{[\text{Gelatin}]_{\text{total}}} * 100$$

Three parallel samples for each tested formulation were analyzed.

2.10.1. Scanning electron microscopy

The internal microstructure of hydrogels was characterized using scanning electron microscopy (SEM). Following crosslinking, the

hydrogels were equilibrated in PBS overnight at 37 °C to attain their equilibrium water content. Subsequently, samples were subjected to three 5-min washes in dH₂O, then frozen at -20 °C and freeze-dried. Freeze-dried specimens were rapidly immersed in liquid nitrogen, fractured, and sputter-coated with gold using a AGB7234 high-resolution sputter coating. SEM imaging of fracture surfaces was performed using a TESCAN VEGA (TESCAN Orsay Holdings, Brno, Czech Republic) SEM platform operated at 5 kV. Image analysis software (ImageJ, National Institutes of Health, Bethesda, MD, USA) was employed to quantify the pore dimensions in cross-sectional images of the samples.

2.11. Cell culture and maintenance

Primary human cardiac fibroblasts isolated from the ventricles of the adult heart (HCFs, PromoCell, Germany) were expanded in cell culture flasks using a complete fibroblast growth medium 3 (FGM-3, PromoCell, Germany) and maintained at 37 °C in humidified atmosphere, 5 % CO₂. H9C2 immortalized cardiomyoblasts derived from embryonic rat heart tissue (H9C2, ATCC, USA) were expanded in cell culture flasks using a growth medium composed of Dulbecco's Modified Eagle Medium (DMEM) (Thermo Fisher Scientific), 10 % Fetal Bovin Serum (FBS, Thermo Fisher Scientific), 1 % sodium pyruvate (Thermo Fisher Scientific), 1 % penicillin/streptomycin (Thermo Fisher Scientific), and 2 % L-glutamine (Thermo Fisher Scientific). To create cell pellets for *in vitro* experiments, cells were washed using PBS, removed from the culture flasks using 0.25 % Trypsin-EDTA (Thermo Fisher Scientific, USA) and cell number was determined using Neubauer chambers. Next, cells were diluted to the desired amount and centrifuged at specific rpm, depending on the cell type (1100 rpm for HCFs and 800 rpm for H9C2).

2.12. Cell viability and morphology

HCFs and H9C2 cells were directly seeded on hydrogel surfaces to evaluate cell viability and morphology. Initially, sterile bio-orthogonal alginate-gelatin hydrogel disks were prepared for 2D cell culture experiments. Briefly, ALG-Az, and GEL-Az lyophilized powders were UV sterilized for 1 h before being dissolved in sterile PBS to prepare stock solution. Meanwhile, the 4-arm-PEG-DBCO stock solution was sterile-filtered through a 0.22 µm syringe filter (Polyethersulfone membrane, Carlo Erba, Italy). Subsequently, ALG-Az and GEL-Az solution was mixed with 4-arm-PEG-DBCO solution and the final solution was quickly poured between two glass plates spaced 500 µm apart. The solution was allowed to react for 30 min. Following gelation, 11 mm disks were punched out and transferred to a 48-well cell culture plate. To obtain double-crosslinked samples (AG_DC), hydrogels were incubated in sterile 0.1 M CaCl₂ for 30 min and washed thrice with PBS. Finally, all samples were incubated in culture medium for at least 12 h before cell seeding. AG_Click and AG_DC bio-orthogonal hydrogels were then cultured with HCFs, seeded at a cell density of 30,000 cells/cm², or H9C2 cells seeded at a cell density of 20,000 cells/cm². After pre-determined time points (24 h and 7 days), cell culture medium was removed and HCFs viability was assessed by incubation with CellTiter-Blue® Cell Viability Assay (Promega, United States) for 3 h. Finally, fluorescence intensity was measured with a plate reader at ex/em = 560/590 nm. Results were reported as the average fluorescence intensity value normalized to the control.

In a parallel experiment, HCFs and H9C2 cells seeded on hydrogels were fixed in paraformaldehyde 4 % w/v% in PBS (PFA, Alfa Aesar) for 30 min, after 7 days culture time. Fixed cells were then stained with Phalloidin Green 488 (Sigma-Aldrich) and nuclei were counterstained with DAPI (Sigma-Aldrich). Samples were visualized using a fluorescence microscope system Nikon Ti2-E (Nikon Instruments, Japan).

2.13. Cell spreading

The influence of substrate elasticity and/or viscoelasticity on HCFs behavior was evaluated through cell spreading experiments using purely elastic polyacrylamide or viscoelastic alginate-gelatin hydrogels as cell adhesion substrates. Bio-orthogonal AG_Click and AG_DC substrates were prepared as described in the previous section. Gelatin-functionalized polyacrylamide hydrogels were prepared adapting to the protocol reported by Karotsu et al. [44]. Precursor solutions were prepared with different concentrations of acrylamide (AAM; Sigma-Aldrich, Italy) and N,N'-methylenebisacrylamide (BIS; Sigma-Aldrich, Italy) to vary elasticity. For conjugation of gelatin from cold water fish skin, 6-acrylamidohehexanoic acid (ACA; BLD Pharmatech Ltd., China) solution (500 mM, pH 7) was added to the AAM-BIS mixture to a final concentration of 100 mM. AAM and BIS concentrations are shown in [Supplementary Table S2](#). Polymerization was initiated with 0.05 % ammonium peroxydisulfate (APS; Sigma-Aldrich, Italy) and catalyzed with 0.2 % N,N,N',N'-tetramethylethylenediamine (TEMED; Sigma-Aldrich, Italy). The polymerizing solutions were gently poured into the gap of slide glasses spaced with a 500 µm silicone membrane. After polymerization, the gels were fully hydrated in 0.1 M 2-(N-morpholino) ethanesulfonic acid (MES) buffer (pH 6.1) overnight. Next, hydrogel disks (11 mm Ø) were punched out. To functionalize hydrogel surface with gelatin, carboxyl groups of the copolymerized ACA were activated with 0.5 M NHS and 0.2 M EDC in 0.1 M MES buffer (pH 6.1) for 30 min at room temperature, washed with cold 60 % methanol/PBS for 2 h at 4 °C, and reacted overnight with 2 % w/v gelatin diluted in PBS at 37 °C. After washing three times with PBS, the hydrogels were placed on the bottom of 48-well cell culture plates and exposed to UV light in a sterile hood for 30 min. Before plating the cells, hydrogels were equilibrated in FGM-3 medium for at least 12 h at 37 °C. HCFs were seeded on hydrogel surfaces at a low density of 10,000 cells/cm², so that they did not contact other cells on average. Cells were allowed to spread for 24 h, and then were fixed and stained for analysis. For measurements of the cell spreading area, images of DAPI/Phalloidin-stained cells were taken using a fluorescence microscope system Nikon Ti2-E (Nikon Instruments, Japan). Only those cells that did not exhibit any cell-cell contacts were considered in the analysis. Images of all single cells were then thresholded manually on the basis of the actin stain, and the area and circularity of the thresholded cell body were determined using ImageJ.

2.14. Live/dead imaging of encapsulated cells

The suitability of developed bio-orthogonal double cross-linked viscoelastic hydrogels for 3D cell culture was evaluated by encapsulating HCFs within hydrogels. Briefly, sterile ALG-Az and GEL-Az were dissolved in sterile Dulbecco's Modified Eagle Medium (DMEM; Thermo Fisher Scientific, United States) to prepare stock solutions. Subsequently, ALG-Az and GEL-Az mixture was mixed with a 50 µL suspension of HCFs to obtain a final cell encapsulation density of 1.5 × 10⁶ cells/mL. The cell-embedding precursor was mixed with 4-arm-PEG-DBCO solution, quickly deposited between two glass plates spaced 500 µm apart and allowed to cross-link for 30 min. Then, disks with 11 mm diameter were punched out and transferred to a low attachment 24-well cell culture plate. Hydrogels were incubated in sterile 0.1 M CaCl₂ solution for 30 min to allow double cross-linking and washed thrice with PBS. Each cell-laden construct was finally cultured in 500 µL of FGM-3 medium. Live (green)/dead (red) staining (Thermo Fisher Scientific, United States) of the cell-laden 3D constructs was performed at 1 h and 24 h after cell encapsulation. At each time point, calcein-AM (live) and ethidium homodimer-1 (dead) were diluted in FGM-3 according to the manufacturer's instructions, added to 3D constructs and incubated for 30 min at room temperature in the dark. The stained cell-laden hydrogels were mounted on a glass bottom dish and imaged using a fluorescence spinning disk microscope system Nikon Ti2-E (Nikon Instruments,

Japan). The composite image was created by overlaying 50 consecutive Z-stack images separated by a distance of 10 μm . The live and dead cells were quantified by using ImageJ.

2.15. Statistical analysis

Results are reported as mean \pm standard deviation (SD). Specific numbers of replicates ($n \geq 3$) are noted for each experiment within the Results section. Statistical significance was determined by performing a two-sided Student's T-test or one-way ANOVA followed by the Tukey's post hoc test for multiple comparisons with significance accepted at $p < 0.05$.

3. Results

3.1. Synthesis and characterization of alginate-azide and gelatin-azide conjugates

Table 2 reports alginate and gelatin intrinsic viscosity and M_n calculated through the Mark-Houwink-Sakurada equation (Supplementary Fig. S1A–B). Notably, gelatin intrinsic viscosity and M_n were measured from gelatin solutions at pH 8, which corresponds to the isoelectric point as assessed by turbidity measurements (Supplementary Fig. S2). ALG-Az and GEL-Az were then prepared through zero-length amidation reaction between the amino groups of Azido-PEG3-amine and the carboxylic groups of alginate and gelatin, exploiting EDC/NHS chemistry (Fig. 1A). The degree of substitution ($DS_{\text{alg}}\%$ and $DS_{\text{gel}}\%$) was calculated to be $10.98 \pm 0.02 \%$ for ALG-Az, following a previously reported grafting protocol [40], and $27.87 \pm 0.07 \%$ for GEL-Az, upon optimizing the quantities of azido-PEG3-amine, EDC and NHS respect to carboxylic acid groups in gelatin (Supplementary Table S1). ATR-FTIR spectra of freeze-dried ALG-Az and GEL-Az samples showed the appearance of a new absorption peak at 2100 cm^{-1} , attributed to azide stretching (Fig. 1B), confirming the successful functionalization. This finding was further confirmed by UV/Vis spectra of ALG-Az and GEL-Az solutions in the presence of DBCO (Fig. 1C): the decreased intensity of the absorption band intensity of free DBCO at 308 nm suggested its partial reaction with azide groups.

The Ca^{2+} ionic crosslinking ability of ALG-Az versus alginate solution was assessed by measuring the diameter (Supplementary Fig. S3A) and circularity (Supplementary Fig. S3B) of microbeads, formed by dropping solutions into a 0.1 M CaCl_2 coagulation bath, by brightfield microscopy analysis. Calcium ion-crosslinking of ALG-Az solution drops caused their gelation into microbeads with lower circularity (0.85 ± 0.03) and higher Feret diameter ($3.01 \pm 0.11 \text{ mm}$) than unmodified alginate microbeads (0.88 ± 0.01 and $2.51 \pm 0.15 \text{ mm}$, respectively), attributed to their lower crosslinking degree.

3.2. Hydrogels design and physical characterization

Bio-orthogonal hydrogels (AG_Click) with two different DBCO:azide molar ratios (R0.5 and R1) were prepared via a catalyst-free SPAAC reaction between ALG-Az and GEL-Az conjugates and 4-arm-PEG-DBCO, dissolved in PBS, leading to triazole bond formation. The actual degree of chemical cross-linking can be precisely assessed by quantifying residual azide groups in the hydrogel network through UV-Vis spectroscopy (Supplementary Fig. S4). Results showed that the effective reacted DBCO:azide molar ratios were 0.37 ± 0.2 and 0.81 ± 0.5 for the

Table 2

Intrinsic viscosity and viscosity-average molecular weight (M_n) of alginate and gelatin.

Sample	Intrinsic viscosity (cm^3/g)	M_n (kDa)
Alginate	1187 ± 78	462 ± 78
Gelatin	14 ± 3	54 ± 13

theoretical R0.5 and R1 formulations, respectively, confirming a high conversion efficiency ($\sim 74 \%$ and $\sim 81 \%$) in both conditions. Bio-orthogonal double cross-linked hydrogels (AG_DC) (Fig. 2) were prepared by additional crosslinking of alginate chains through calcium ions.

3.2.1. Hydrogel formation and viscoelastic properties

Rheological studies were performed to analyze hydrogels formation and determine their viscoelastic response. Time sweep tests of hydrogels precursors were performed to inform on the kinetics of SPAAC-mediated cross-linking: for all tested formulations, the storage modulus (G') rapidly increased reaching a plateau value in about 20 min (Supplementary Fig. S5A). AG_Click(R1) hydrogels exhibited a shorter cross-over (i.e., $G' = G''$) time ($112 \pm 34 \text{ s}$) compared to AG_Click(R0.5) hydrogels ($192 \pm 72 \text{ s}$), and a higher G' plateau value, attributed to the higher DBCO:azide ratio and higher cross-linking density of the formers (Supplementary Fig. S5B). Frequency sweep tests showed that hydrogels displayed a predominantly elastic behavior ($G' > G''$) across frequencies from 1 to 100 rad/s (Fig. 3A). The Young's modulus (E), derived from G' and G'' values at 1 Hz (i.e., 6.28 rad/s), increased as a function of DBCO:azide ratio, from $1.5 \pm 0.2 \text{ kPa}$ for AG_Click(R0.5) to $7.6 \pm 1.1 \text{ kPa}$ for AG_Click(R1), suggesting an increase in cross-linking density. Particularly, stiffness of AG_Click(R1) closely matched the one reported for native cardiac tissue ($\sim 10\text{--}30 \text{ kPa}$) (Fig. 3B) [24]. The addition of ionic cross-linking significantly increased the elastic modulus of AG_DC(R0.5) hydrogel, reaching a value of $3.8 \pm 0.1 \text{ kPa}$, while had a negligible effect on the stiffness of AG_DC(R1) samples ($7.7 \pm 0.8 \text{ kPa}$). The loss tangent ($\tan \delta = G''/G'$) at 1 Hz provides an indication on viscoelastic properties. As shown in Supplementary Fig. S6, AG_Click(R0.5) hydrogels showed higher $\tan \delta$ values (0.06 ± 0.03) than AG_Click(R1) hydrogels (0.005 ± 0.002). Double cross-linking increased the loss tangent of AG_DC(R1) hydrogels (0.019 ± 0.005) respect to AG_Click(R1) samples (0.005 ± 0.002) while did not significantly affect the loss tangent of AG_DC(R0.5) versus AG_Click(R0.5) hydrogels. Further insights on the viscous stress dissipation, determining viscoelastic properties of hydrogels, were gathered by shear stress relaxation tests (Fig. 3C). Chemically cross-linked polyacrylamide hydrogels with a prevalent elastic response and negligible stress relaxation were tested as a reference. Bio-orthogonal alginate-gelatin hydrogels exhibited viscous stress dissipation mediated by their dynamic viscoelastic network, showing a decrease in shear stress over time (Fig. 3C). Notably, AG_Click(R0.5) had a faster relaxation time ($\tau_{1/2}$; $280 \pm 74 \text{ s}$) compared to AG_Click(R1) ($598 \pm 92 \text{ s}$), as an effect of the lower cross-linking degree. The addition of reversible ionic interactions to get double cross-linked hydrogels significantly reduced $\tau_{1/2}$ for both AG_DC(R0.5) ($154 \pm 10 \text{ s}$) and AG_DC(R1) ($273 \pm 33 \text{ s}$).

3.2.2. Physicochemical properties and microstructure

The swelling and degradation behavior of AG_Click and AG_DC hydrogels was monitored over 28 days in PBS (pH 7.4, 37°C) and in PBS supplemented with type II collagenase (2.5 U/mL). As shown in Fig. 4A, AG_Click(R0.5) hydrogels exhibited a progressive swelling increase from $82 \pm 7 \%$ at day 1 to a peak of $138 \pm 8 \%$ at day 21, followed by a slight reduction to $62 \pm 17 \%$ at day 28 in PBS. When incubated in collagenase, AG_Click(R0.5) hydrogels showed higher initial swelling ($100 \pm 6 \%$ at day 1), but underwent complete degradation within 7 days. AG_Click(R1) hydrogels displayed a lower swelling percentage at day 1 ($57 \pm 0.4 \%$), which remained stable up to day 28 in PBS ($51 \pm 8 \%$), while in collagenase they showed a maximum swelling of $114 \pm 8 \%$ at day 7, followed by a progressive degradation, reaching a $72 \pm 10 \%$ weight loss at day 28.

Double cross-linked hydrogels initially presented reduced swelling compared to AG_Click samples, with differences progressively decreasing in PBS over time, and showed enhanced stability in the presence of collagenase. AG_DC(R0.5) hydrogels reached a swelling percentage of $135 \pm 12 \%$ at day 21 in PBS, slightly decreasing to $64 \pm 10 \%$ at day 28. In collagenase, they displayed a maximum swelling of

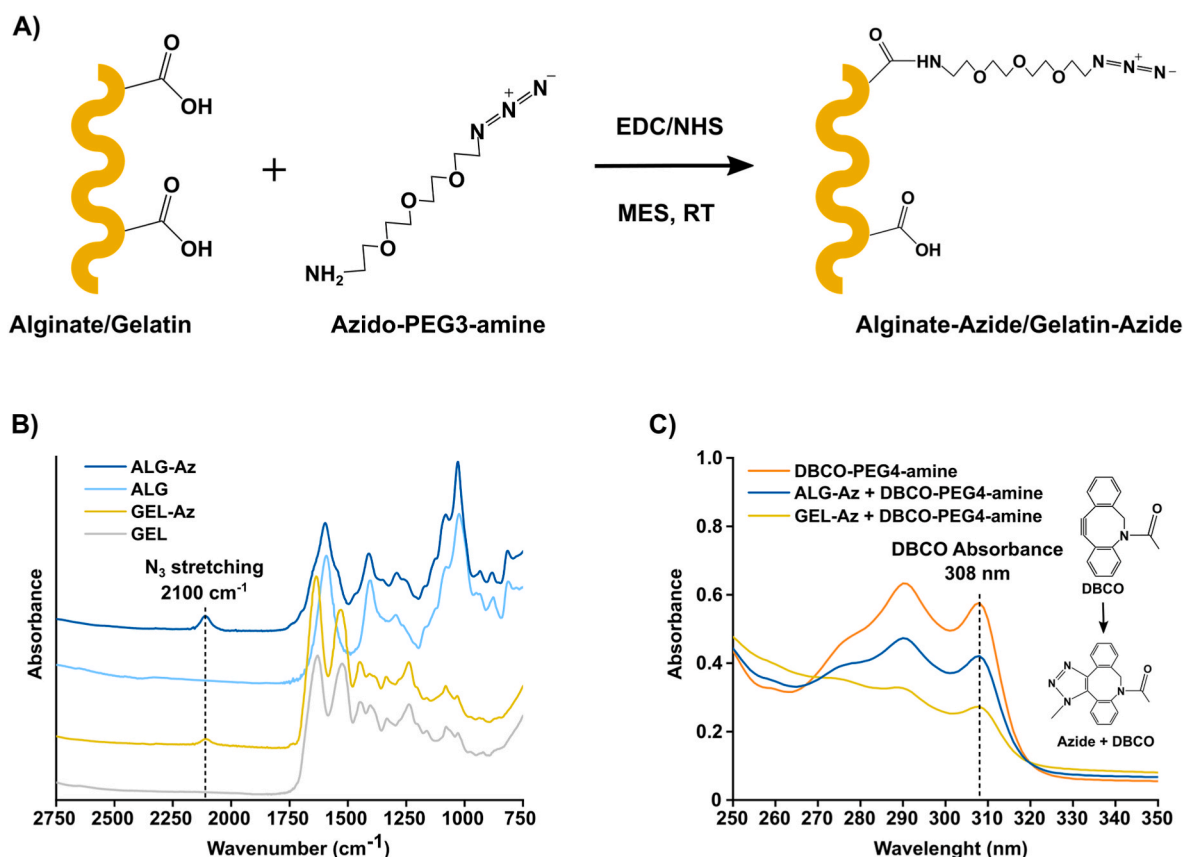


Fig. 1. Synthesis and characterization of alginate-azide and gelatin-azide conjugates. (A) Reaction scheme of azido-PEG3-amine conjugation on available carboxyl groups of alginate and gelatin through EDC/NHS coupling in MES buffer at room temperature. (B) ATR-FTIR spectra of freeze-dried ALG-Az and GEL-Az compared to alginate and gelatin powders in the 2750–750 cm^{-1} wavenumber range. (C) UV-Vis spectra in the 250–350 nm wavelength range of DBCO-PEG4-amine, ALG-Az + DBCO-PEG4-amine and GEL-Az + DBCO-PEG4-amine solutions. The amount of azide groups in ALG-Az and GEL-Az was quantified through the decrease of the absorbance intensity band of DBCO-PEG4-amine at 308 nm.

141 \pm 11 % at day 7, then gradually degraded with complete weight loss within 21 days. AG_DC(R1) hydrogels showed minimal swelling at day 1 (35 \pm 1 %), which progressively increased to 63 \pm 6 % by day 21 in PBS, and remained stable. Under collagenase conditions, these hydrogels reached a maximum swelling of 82 \pm 13 % at day 7, followed by a controlled degradation, resulting in 58 \pm 10 % weight loss by day 28.

The microstructure of the AG_Click and AG_DC hydrogels was analyzed to evaluate the impact of different cross-linking strategies. Supplementary Fig. S7 shows SEM images of fractured sections of the freeze-dried hydrogels. AG_Click(R0.5) (Fig. S7A) exhibited a more porous structure with larger and interconnected pores compared to the more densely packed structure of AG_Click(R1) hydrogel (Fig. S7C), where slightly smaller pores were observed, consistent with its higher cross-linking degree. The double cross-linked AG_DC formulations (Fig. S7B and S7D) showed a slightly denser pore network compared to AG_Click samples.

3.3. Culture tests with human cardiac fibroblasts

3.3.1. Hydrogels biocompatibility and substrate-mediated cell spreading

To assess the potential of the developed bio-orthogonal alginate-gelatin hydrogels to be exploited as scaffolds for cardiac tissue engineering, their *in vitro* cytocompatibility and ability to promote cell adhesion were studied using HCFs and H9C2 rat cardiomyoblasts. Cytocompatibility was evaluated following ISO 10993-5 guidelines through a direct contact test, with HCFs directly cultured on the hydrogel sample surface. As shown in Fig. 5A, viability of HCFs cultured on chemically cross-linked and double cross-linked hydrogel sample surface was higher than 80 % compared to control conditions (i.e. cells

cultured on standard 2D cell culture plates) and showed a slight increase from 1 to 7 day-culture time. Interestingly, HCF viability on AG_DC(R1) samples achieved the highest values (>100 %). Immunofluorescence analysis of both HCFs (Fig. 5B) and H9C2 cells (Supplementary Fig. S8) by nuclei/F-Actin staining after 7 days culture showed that the hydrogels supported cell attachment and spreading of different types of cardiac cells. In order to test the effect of hydrogel stiffness and viscoelasticity on HCF behavior, the spreading area of HCFs cultured at low-density (10000 cells/ cm^2) on viscoelastic bio-orthogonal alginate-gelatin hydrogels and control elastic hydrogels, based on gelatin-functionalized polyacrylamide with low (pAAM_LS, 2 kPa) and high stiffness (pAAM_HS, 8 kPa), was assessed. The spreading area of isolated cells was measured to avoid the influence of cell-cell contact, through phalloidin staining of F-actin filaments. As shown in Fig. 5C, cell spreading area was higher on elastic pAAM_HS gels ($E \sim 8$ kPa) compared to pAAM_LS gels ($E \sim 2$ kPa), where HCFs showed a prevalently rounded shape (1321 \pm 403 μm^2 versus 727 \pm 325 μm^2 , respectively). Stress-relaxing soft AG_Click(R0.5) hydrogels ($E \sim 2$ kPa; $\tau_{1/2}$ –280 s) promoted cell elongation and significantly higher cell spreading area (898 \pm 394 μm^2) compared to elastic pAAM_LS hydrogels. On the other hand, cells on AG_DC(R0.5) hydrogels, which displayed both increased stiffness and relaxation ($E \sim 4$ kPa; $\tau_{1/2}$ –154 s), exhibited a slightly reduced spreading area (848 \pm 325 μm^2). Finally, concerning the stiffer viscoelastic formulations, both AG_Click(R1) ($E \sim 8$ kPa; $\tau_{1/2}$ –598 s) and AG_DC(R1) ($E \sim 8$ kPa; $\tau_{1/2}$ –270 s) promoted cell elongation with higher cell spreading areas of 904 \pm 492 μm^2 and 940 \pm 460 μm^2 , respectively, compared to the soft viscoelastic hydrogels. Conversely, cells on stiff, stress-relaxing hydrogels exhibited a significantly lower spreading area compared to the elastic pAAM_HS control

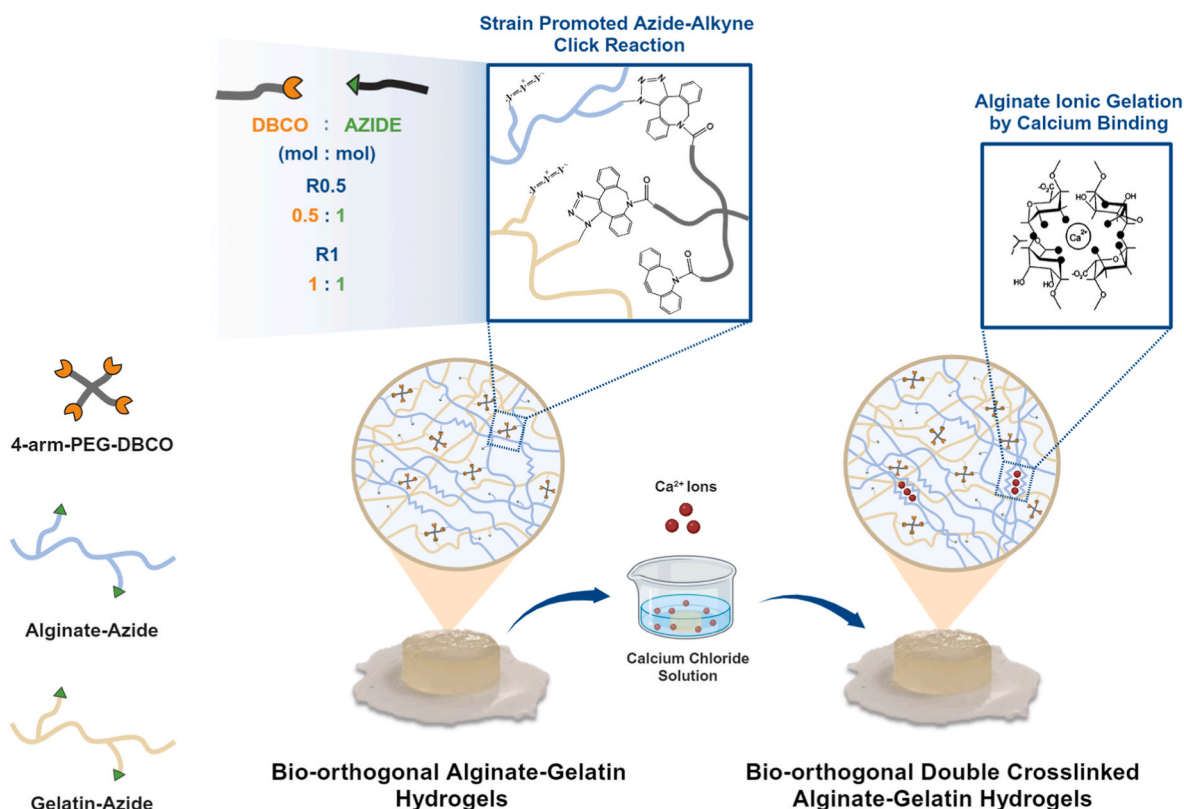


Fig. 2. Design of bio-orthogonal viscoelastic alginate-gelatin hydrogels. Bio-orthogonal hydrogels were prepared via a catalyst-free strain-promoted azide-alkyne click reaction (SPAAC) between azides groups on ALG-Az and GEL-Az, with DBCO end groups of a 4-arm cross-linker (4-arm-PEG-DBCO). Double cross-linked hydrogels were obtained by further calcium ionic crosslinking of alginate strands in chemically cross-linked hydrogels.

gels, but with a more asymmetrically elongated shape as demonstrated by reduced cell circularities (Supplementary Fig. S8).

3.3.2. Cell encapsulation

To evaluate the suitability of the developed bio-orthogonal alginate-gelatin hydrogels for 3D cell cultures, HCFs were encapsulated within AG_DC(R1) hydrogel. This formulation was selected based on its biomimetic properties, such as cardiac tissue-like stress relaxation and stiffness. As shown in Fig. 6, encapsulated HCFs exhibited high viability (>85 %) when cultured for 1, 3, and 7 days within the hydrogel, as assessed by Live/Dead assay.

4. Discussion

The design of biomimetic hydrogels able to replicate the dynamic viscoelastic properties of the native myocardium represents a major challenge in cardiac tissue engineering [4,45,46]. Indeed, hydrogels have been commonly designed to replicate cardiac tissue-like stiffness only, failing to reproduce the typical heart stress relaxation behavior [11,47]. Another concern in hydrogel design has been the adoption of potentially cytotoxic cross-linking methods, which may interfere with the biological environment. Recent advances in bio-orthogonal cross-linking reactions have provided new approaches for rapid and cell-friendly cross-linking of hydrogels under physiological conditions [48]. Additionally, chemical and ionic double cross-linking has been proposed to improve hydrogel stability and achieve tunable viscoelastic properties of alginate hydrogels, which are among the most investigated for cardiac regeneration [49–51]. Furthermore, the lack of bioactivity in alginate hydrogels has been frequently addressed by the incorporation of gelatin, which provides RGD motifs to promote cell adhesion and proliferation while retaining alginate structural benefits [52,53].

In this study, we designed novel double cross-linked alginate-gelatin

hydrogels through bio-orthogonal SPAAC chemistry and calcium ion cross-linking for next exploitation in cardiac tissue engineering. This approach uniquely combined the tunable viscoelastic properties of double cross-linked alginate network with the bioactivity of gelatin, highlighting the role of viscoelasticity on 2D cell attachment and spreading of HCFs and providing a cell-friendly approach for perspective 3D cell cultures.

The controlled chemical functionalization of alginate and gelatin was crucial for hydrogel development. Due to batch-to-batch variability of natural polymers, we first characterized their molecular weights (462 kDa for alginate and 54 kDa for gelatin) to ensure consistency in experiments [54,55]. For the synthesis of ALG-Az, we employed the EDC/NHS coupling protocol reported by Moody and co-authors [40], achieving a degree of substitution of ~11 %, without impairing the ionic cross-linking capacity of alginate. GEL-Az was prepared by a green organic-free EDC/NHS coupling reaction, which represents an advancement compared to previously reported methods making use of organic solvents [56]. The degree of substitution of GEL-Az (~28 %) was optimized to ensure effective incorporation of azide functionalities while maintaining gelatin bioactivity. Subsequently, for hydrogels development, ALG-Az/GEL-Az 20/80 (w/w) composition was selected to balance gelatin bioactivity and alginate structural support [53,57,58]. The addition of 4-arm-PEG-DBCO to ALG-Az and GEL-Az containing solutions at two different DBCO:azide molar ratios (R0.5 and R1) allowed SPAAC-mediated cross-linking, with complete gelation in approximately 20 min. UV-Vis analysis confirmed efficient cross-linking, with effective reacted ratios of 0.37 and 0.81 for R0.5 and R1, respectively, supporting the ability to modulate network density via formulation design. Gelation was faster compared to previously developed alginate-based hydrogels cross-linked through other bio-orthogonal approaches, such as the Diels-Alder reaction, which takes hours to reach completion [12]. The quick and efficient SPAAC

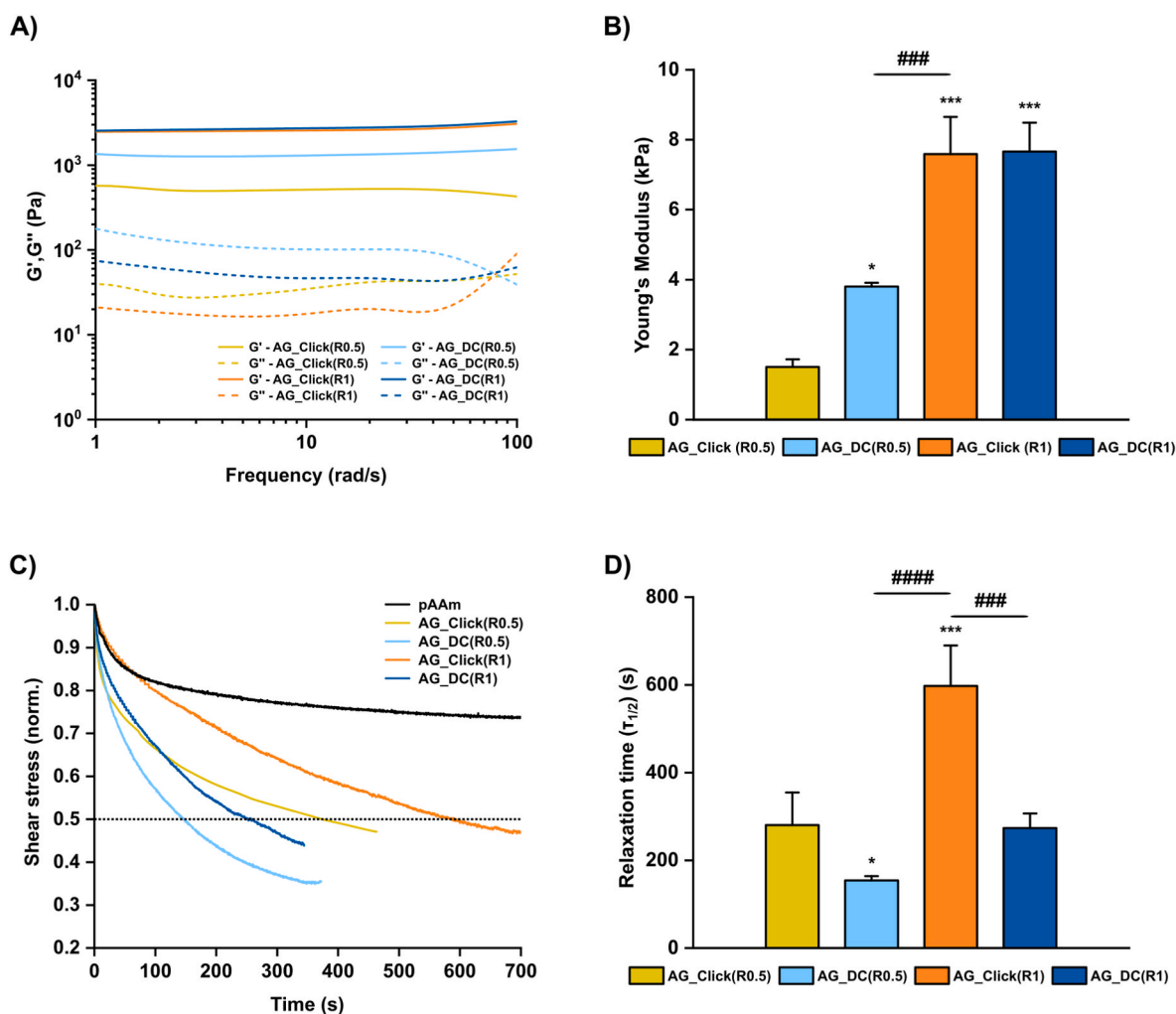


Fig. 3. Rheological characterization of alginate-gelatin hydrogels. (A) Storage modulus (G' , continuous line) and loss modulus (G'' , dotted line) of alginate-gelatin hydrogels (AG) as a function of angular frequency ($n = 3$). (B) Young's Moduli (kPa) calculated from G' and G'' values at 1 Hz in (A), as previously reported [42] ($n = 3$). (C) Shear stress relaxation of alginate-gelatin hydrogels and polyacrylamide hydrogels (pAAm) as elastic control samples ($n = 3$). (D) Relaxation time ($\tau_{1/2}$), i.e., the time at which the shear stress relaxed to half of its original value, derived from stress relaxation tests in (C) ($n = 3$). Statistical differences between the groups were determined with one-way ANOVA followed by the Tukey's post hoc test for multiple comparisons. (*) refers to AG_Click (R0.5) comparisons, (#) includes all other comparisons. * $p < 0.05$, ** $p < 0.01$, *** $p < 0.001$. #### $p < 0.001$, ##### $p < 0.0001$.

reaction is advantageous for a variety of biomedical applications, including injectable hydrogels with/without 3D cell encapsulation and/or bioprinting, where prolonged cross-linking times could negatively impact cell viability and/or the material supporting properties [31,59]. Although SPAAC chemistry offers remarkable selectivity and cytocompatibility, the use of strained cyclooctynes such as DBCO can still be limited by their synthetic complexity and cost. However, recent studies have reported increasingly efficient and scalable synthetic routes for these moieties, supporting their future large-scale applicability in translational contexts [60,61]. By tuning the molar ratio of DBCO:Azide (R0.5 and R1), we achieved not only rapid cross-linking but also the ability to finely tune the network viscoelastic properties. Controlling the stiffness of hydrogels is crucial in tissue engineering, as it significantly impacts cell adhesion, migration, and differentiation [11,44,62,63]. The frequency sweep tests (Fig. 3A) showed that all formulations exhibited predominantly elastic behavior ($G' > G''$) across a range of frequencies (1–100 rad/s), confirming the efficiency of the SPAAC reaction in forming a stable hydrogel network [18,31,64,65]. Rheological analysis also showed that increasing DBCO:Azide ratio from 0.5 to 1 enhanced hydrogel stiffness, as evaluated through the Young's modulus (Fig. 3B), from ~2 kPa for AG_Click(R0.5) to ~8 kPa for AG_Click(R1), thereby reaching similar values to those reported for cardiac tissue (~10 kPa

[62,66]. Changes in stiffness were attributed to a different cross-linking degree of the hydrogel samples.

The introduction of double ionic and covalent cross-linking impacted the mechanical properties, particularly of AG_DC(R0.5) hydrogels, leading to a significant increase in the elastic modulus (~4 kPa) compared to chemically cross-linked AG_Click(R0.5) hydrogels (~2 kPa) (Fig. 3B). This effect was less pronounced in the AG_DC(R1) formulation, suggesting that the contribution of ionic cross-links was more substantial in the hydrogel with lower chemical cross-linking density. Conversely, in AG_DC(R1) formulation, the covalent network dominated the elastic response, limiting the influence of additional ionic cross-linking. However, in both AG_DC(R1) and AG_DC(R0.5) hydrogels, ionic cross-linking enhanced the viscoelastic behavior, by increasing loss tangent values ($\delta = G''/G'$; Supplementary Fig. S5). AG_DC(R1) hydrogels resulted particularly interesting as their stiffness and viscoelasticity could be separately tuned through chemical and ionic cross-linking respectively, to mimic the dynamic mechanical response of cardiac tissue [12,64]. Indeed, while most research in cardiac tissue engineering has been focused on tailoring hydrogel stiffness only, recent studies have highlighted the importance of viscoelasticity response in influencing key cellular processes, such as cell spreading, cytoskeletal organization, differentiation and ECM remodeling [8–10]. Hence, in this work, the

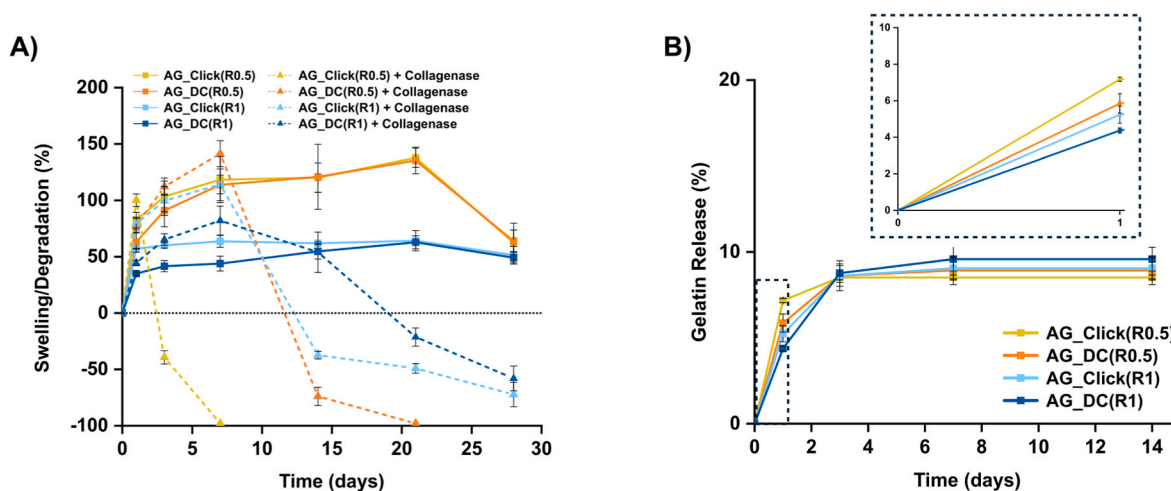


Fig. 4. Physicochemical properties of alginate-gelatin hydrogels. (A) Swelling/degradation percentage of AG_Click and AG_DC hydrogels incubated in PBS and PBS with type II collagenase (2.5 U/mL) at 37 °C for up to 28 days (n = 3). Positive values indicate swelling, while negative values correspond to weight loss due to degradation. (B) Cumulative gelatin release (wt%) from hydrogels after 1, 3, 7 and 14 days in PBS at 37 °C (n = 3). Percentages are referred to the total amount of gelatin within the samples.

stress relaxation properties of alginate-gelatin hydrogels were systematically evaluated to investigate their potential for mimicking the mechanical properties of cardiac ECM (Fig. 3C and D). Polyacrylamide hydrogels (pAAm) were chosen as reference pure elastic materials, having predominant elastic response and minimal stress relaxation [11]. All tested alginate-gelatin hydrogels exhibited viscoelastic properties with stress relaxation response over time, including chemically cross-linked AG_Click hydrogels. Indeed, chemical cross-linking through SPAAC reaction contributed to the formation of stable covalent bonds, which are critical for hydrogel elastic properties, preventing plastic deformation under stress. However, the resulting covalent hydrogels retained the inherent viscoelastic properties of natural polymers, particularly of gelatin, with chain segments between cross-links undergoing unfolding and conformational changes under mechanical stress, allowing for energy dissipation [6,67–69]. Particularly, the low functionalization degree of both alginate ($DS_{alg} \sim 11\%$) and gelatin ($DS_{gel} \sim 28\%$) with azide groups exposed through PEG spacers and the use of a cross-linking agent with flexible PEG segments end-functionalized with reactive DBCO (4-arm-PEG3-DBCO) together contributed to modulate the hydrogel network mesh size, leading to long and flexible chain segments among the cross-links. Indeed, previous studies have shown that lower cross-linking density of flexible polymer chains enhances stress relaxation [67,69] and causes faster viscous dissipation [11,70]. Finally, the introduction of ionic cross-linking in AG_DC formulations further amplified the stress relaxation response, thanks to the “zipping-unzipping” mechanisms of calcium ions by alginate strands under shear stress [11,12]. This was particularly evident for AG_DC(R0.5) formulations where the less densely cross-linked network allowed for higher diffusion of calcium ions, strengthening the role of ionic interactions in stress relaxation. However, the external ionic cross-linking method herein employed, based on diffusion, lacks precise control over calcium ion concentration. Future studies will address this limitation obtaining more controlled and homogeneous ionic interactions through an internal cross-linking mechanism making use of calcium sulfate or calcium carbonate [11,71].

Alginate-gelatin hydrogels demonstrated structural stability under physiological-like conditions up to 28 days (PBS, 37 °C), with additional presence of collagenase to simulate enzymatic degradation (Fig. 4A). Swelling and degradation behavior was dependent on cross-linking degree: AG_Click(R0.5) showed progressive swelling until day 21, then a reduction of wet weight by day 28, likely due to mild hydrolytic degradation of gelatin chains partially stabilized by the covalently cross-linked alginate [56,72]. AG_Click(R1) instead maintained nearly

constant weight throughout, confirming the stabilizing effect of higher cross-linking density. AG_DC samples showed reduced swelling in PBS initially, but converged to values similar to AG_Click beyond 14 days, suggesting progressive calcium ion leaching. Nevertheless, calcium ions improved long-term stability and delayed degradation in collagenase, especially within the first 7–14 days. These observations support the importance of double cross-linking in stabilizing the network, while highlighting the limitations of external ionic cross-linking, which is prone to ion diffusion. Overall, these results confirm that double cross-linked hydrogels provided an effective stability under physiological conditions and controlled enzymatic degradability, which are crucial for *in vivo* applications in cardiac tissue engineering. Furthermore, other studies have proposed 4-arm-PEG-DBCO cross-linkers incorporating hydrolysable or photodegradable sequences, which could also be exploited in this system to introduce an additional dynamic control on network degradation [56,73]. Hydrogel cross-linking via SPAAC reaction caused the release of only a low fraction of un-reacted gelatin (<10 %) (Fig. 4) during incubation in PBS, demonstrating the efficient and stable incorporation of bioactive gelatin within the hydrogel networks. SEM microstructural analysis of samples (Supplementary Fig. S7) was performed upon hydrogel dehydration through freeze-drying. Although freeze-drying alters the substrate morphology by introducing microporosities through ice crystal sublimation, SEM analysis could provide an indication on the presence of an adequate porous volume within the original hydrogels to favor nutrient and oxygen diffusion.

Once demonstrated the ability of bio-orthogonal alginate-gelatin hydrogels to mimic the viscoelasticity of cardiac ECM microenvironment and their adequate stability in physiological-like conditions, biological investigations were performed by the 2D culture of HCFs and H9C2 cardiomyoblasts. Cardiac fibroblasts were selected as they are highly mechanosensitive and play a fundamental role in myocardial homeostasis and repair by responding to biochemical and mechanical cues of the surrounding matrix [63]. All hydrogel formulations supported HCFs viability (Fig. 5A) and spreading (Fig. 5B), attributed to the bioactivity of gelatin, the main hydrogel component (80 % of the total composition) [53,66]. AG_Click(R1) and AG_DC(R1) showed enhanced ability to support HCF culture, attributed to their additional biomimetic stiffness (~ 8 kPa). The observed cell viability and spreading were further confirmed using H9C2 cardiomyoblasts, which successfully adhered and elongated on AG_DC(R1) hydrogels (Supplementary Fig. S9), highlighting the cytocompatibility of the system for different types of cardiac cells. Most mechanotransduction studies presented in

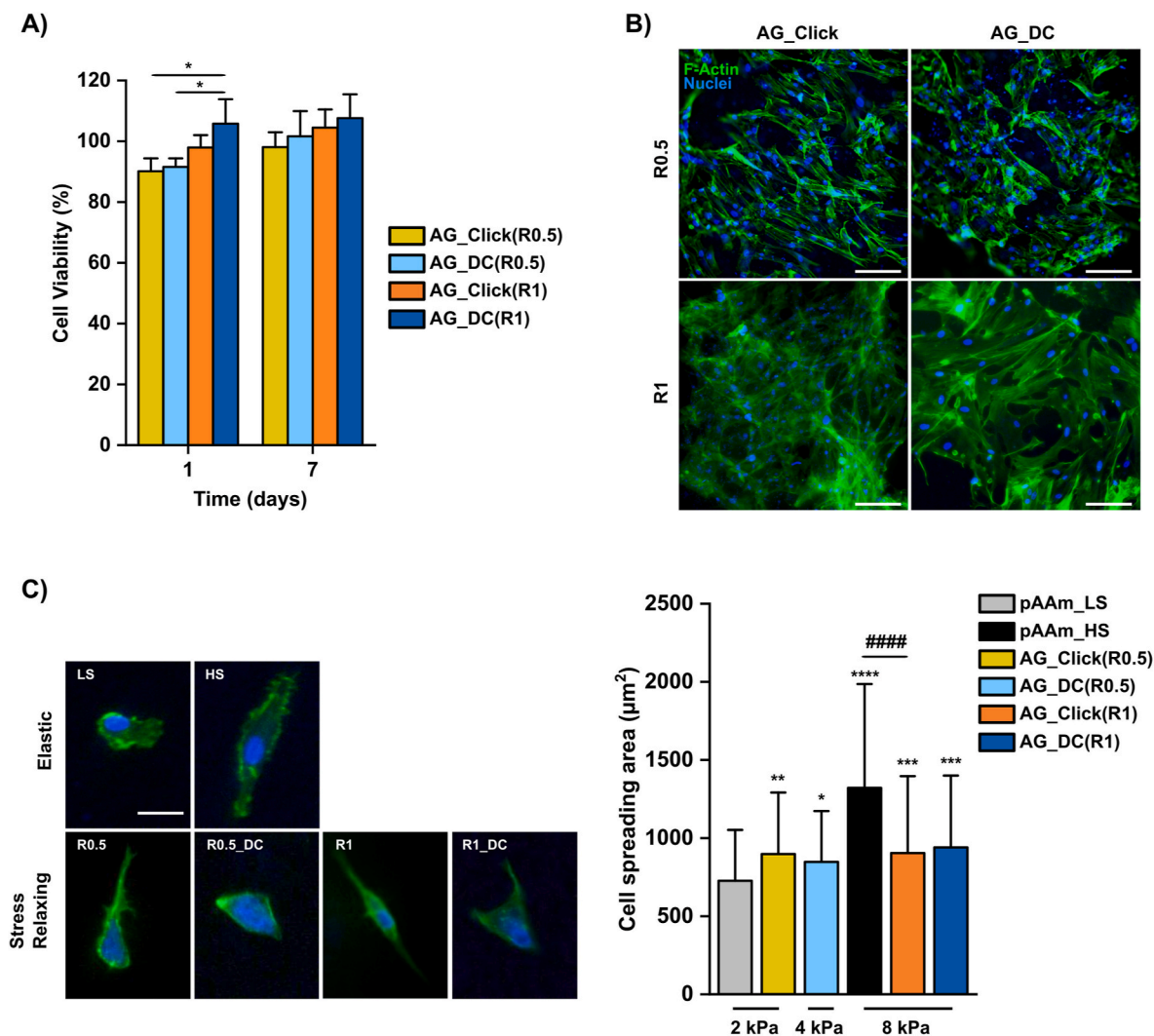


Fig. 5. *In vitro* hydrogels biocompatibility and substrate-mediated cell spreading. (A) Direct cytocompatibility tests of human cardiac fibroblasts (HCFs), evaluated at 24 h and 7 days by 2D seeding on hydrogels. Controls are represented by cells cultured in a standard tissue culture plate ($n = 3$). (B) Nuclei/F-actin staining of HCFs at 7 days for adhesion and morphological evaluation (scale bars = 100 μm). (C) On the left, representative images of cells plated on different hydrogels, taken after 24 h. Actin is depicted in green; the nucleus is depicted in blue (scale bar = 25 μm). On the right, quantification of HCFs cell-spreading area as a function of hydrogels elastic modulus for cells on low stiffness elastic (pAAm_LS), high stiffness elastic (pAAm_HS) or stress-relaxing (AG) substrates ($n = 58$ –122). Statistical differences between the groups were determined with one-way ANOVA followed by the Tukey's post hoc test for multiple comparisons. (*) refers to pAAm_LS comparisons, (#) includes all other comparisons. * $p < 0.05$, ** $p < 0.01$, *** $p < 0.001$, **** $p < 0.0001$. #### $p < 0.0001$.

literature, have investigated the influence of substrate viscoelasticity on mesenchymal stem cells (MSCs) behavior and differentiation [11,21]. Similar studies are currently missing in cardiac tissue engineering, highlighting the novelty of the present study in addressing a significant gap in cardiac tissue engineering. Particularly, understanding HCF responses to viscoelastic substrates could provide important insights into their proper design [63]. Low-density cultures of HCFs on hydrogels revealed important insights into how substrate stiffness and viscoelasticity mediated cell spreading (Fig. 5C). Polyacrylamide gels (pAAm) with cardiac tissue-like stiffness and coated with Matrigel were previously reported by Kurotsu and co-workers [44] and herein exploited as control elastic substrates following their functionalization with gelatin instead of Matrigel. As expected, HCF spreading was enhanced in stiffer hydrogels, such as pAAm_HS (8 kPa) and both AG_Click(R1) and AG_DC(R1) hydrogels rather than on soft pAAm_LS (2 kPa), where rounded cells were instead observed, attributed to a reduction in actomyosin traction force on the soft substrates [10,74,75]. On the other hand, soft AG_Click(R0.5) (~2 kPa) promoted significantly greater cell spreading than soft pAAm_LS, attributed to their stress-relaxation properties. This result

supports recent findings showing that viscoelastic substrates allow cells to more effectively yield and remodel their surrounding matrix, and to elongate, even in the absence of biomimetic stiffness [10,11]. While stress relaxation enhanced cell spreading on soft AG_Click(R0.5) hydrogels, higher stiffness of double cross-linked AG_DC(R0.5) hydrogels (~4 kPa) could slightly improve cell elongation, although with a minimal effect on spreading. The effect of stiffness and viscoelasticity on cell behavior was even more evident by comparing stiff elastic pAAm_HS and stiff stress relaxing AG_Click(R1) and AG_DC(R1) hydrogels. In agreement with previous findings, the biomimetic stiffness and stress-relaxation behavior of AG_Click(R1) and AG_DC(R1) hydrogels synergistically contributed to support cellular response compared to pAAm_HS hydrogels [10,70]. As shown by single-cell snippets in Fig. 5C, cells on stiff stress relaxing AG_Click(R1) and AG_DC(R1) hydrogels showed reduced cell spreading area but increased elongation, with spindle-like morphologies (quantified in terms of reduced circularity (Supplementary Fig. S9), compared to cells cultured on purely elastic substrates. These results indicated that while cell spreading is critical for actin organization, elongation can occur independently, with cells

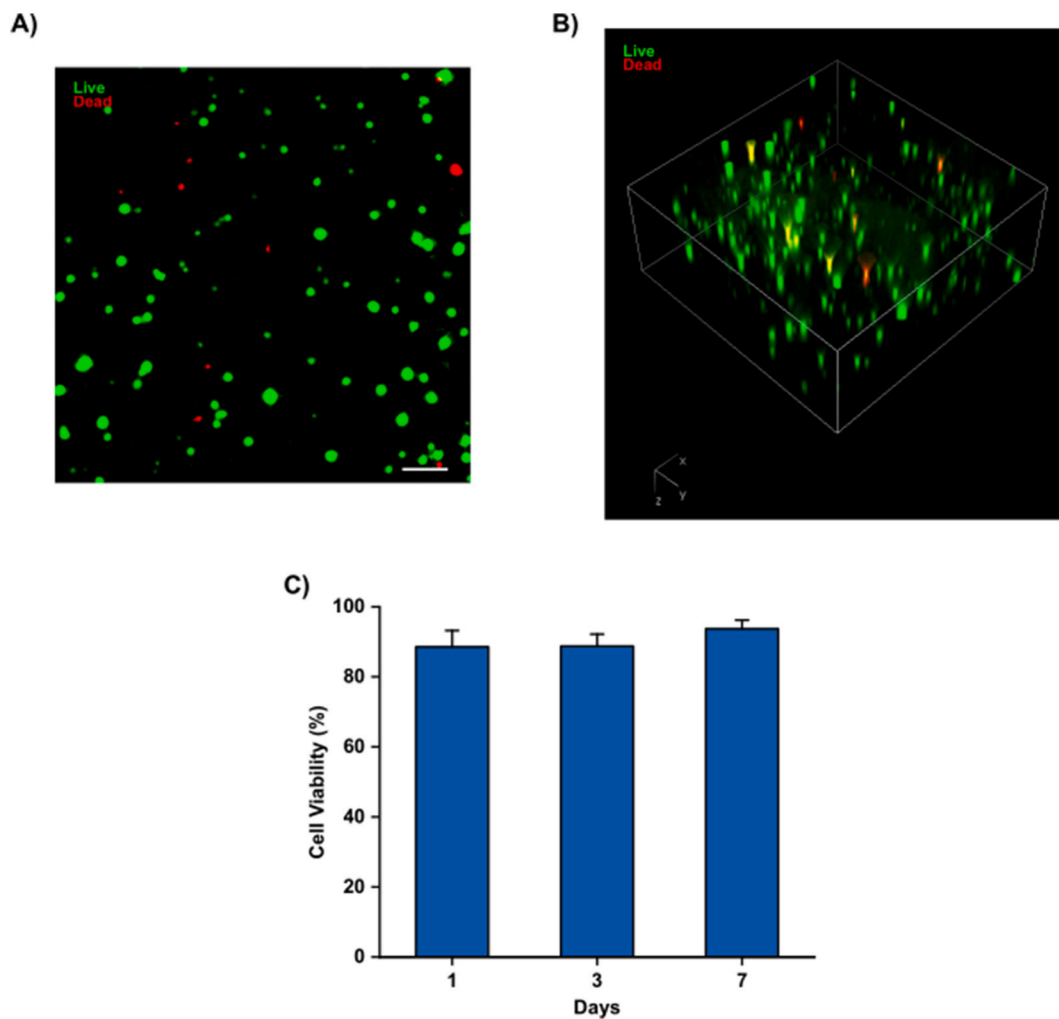


Fig. 6. Live/Dead assay on 3D HCF culture within AG_DC(R1) hydrogels. Fluorescence microscopy (A) maximum intensity projection and (B) volumetric distribution images of Live/Dead assay at 1 day of culture (scale bar: 100 μ m). (C) Cell viability percentage by Live/Dead assay at 1, 3 and 7 days of culture (n = 3).

adopting an elongated morphology without necessarily increasing their area [76,77]. Indeed, previous studies showed how viscoelastic matrices can lead to morphological instability and break the spherical symmetry of cells compared to elastic substrates where cells increase in size maintaining higher circularity [78]. Although results from this work suggested a viscoelasticity-mediated response of HCFs, future investigations will be performed to clarify the underlying cellular mechanisms by studying specific pathways with well-known roles in mechanosensing, such as yes-associated protein (YAP) and the transcriptional coactivator with PDZ-binding motif (TAZ) activation.

Another key advantage of herein developed hydrogels, based on bio-orthogonal SPAAC chemistry, was their ability to support not only 2D cell culture but also 3D cell encapsulation. Particularly, the rapid gelation kinetics and minimal toxicity of SPAAC chemistry make such hydrogels promising for next exploitation as injectable hydrogels and/or engineered cardiac tissues [31,79]. As a proof-of-concept study, herein we investigated 3D cell culture on AG_DC(R1) hydrogel, due to its biomimetic properties for cardiac tissue engineering. HCFs were easily and uniformly encapsulated within AG_DC(R1) hydrogel and displayed high viability after 7 day culture time (Fig. 6). Future research will be addressed to study the behavior of other encapsulated cardiac cells, such as induced pluripotent stem cells-derived cardiomyocytes and/or their co-cultures with HCFs, optimizing cell density and maturation times to support cardiac tissue engineering.

5. Conclusions

In this study, novel bio-orthogonal double cross-linked alginate-gelatin hydrogels were developed with tunable viscoelastic properties, tailored for cardiac tissue engineering applications. Alginate-azide and gelatin-azide conjugates were first obtained and then mixed with 4-arm-PEG-DBCO, enabling hydrogel formation via bio-orthogonal SPAAC chemical cross-linking. Further ionic cross-linking of alginate chains allowed to obtain double cross-linked hydrogels. Hydrogel mechanical properties were thus modulated by varying DBCO:azide molar ratios between 0.5 and 1, with/without further addition of calcium ions. Resulting hydrogel stiffness was found to mainly depend on chemical cross-linking, and was only slightly affected by ionic cross-linking in hydrogels with low chemical cross-linking density (i.e., formulations obtained at DBCO:azide molar ratio equal to 0.5). On the other hand, hydrogel stress relaxation behavior was found to depend both on chemical cross-linking degree (i.e. DBCO:azide molar ratio) and ionic cross-linking, which further enhanced viscoelasticity through the so-called “zipping-unzipping” mechanism of calcium ions.

HCFs cultured on the surface of hydrogel samples showed a viscoelastic-dependent response: HCF adhesion was best supported by hydrogels with biomimetic stiffness (~8 kPa). Stress relaxing hydrogels promoted cell spreading on substrates with low stiffness, while reduced spreading area but increased asymmetric cell elongation was found on high stress relaxing hydrogels with biomimetic stiffness. AG_DC(R1)

hydrogel was found to closely mimic the dynamic viscoelastic properties of cardiac ECM, well supporting HCF viability and spreading. Proof of concept studies demonstrated the viability of HCFs, 3D encapsulated within AG_DC(R1) hydrogel for 7 days.

Findings from this study highlighted the versatility of developed hydrogels in replicating cardiac tissue-like viscoelastic properties, paving the way towards their use as injectable formulations and/or bioprinted substrates for cardiac tissue engineering.

Future studies will explore specific cell mechanotransduction pathways, such as YAP/TAZ activation, to provide more insights on the role of viscoelasticity in guiding cardiac cellular behavior.

CRedit authorship contribution statement

Daniele Testore: Writing – original draft, Visualization, Validation, Methodology, Investigation, Formal analysis, Data curation, Conceptualization. **Alice Zoso:** Writing – review & editing, Visualization, Validation, Supervision, Formal analysis, Conceptualization. **Camilla Paoletti:** Writing – review & editing, Visualization, Validation, Supervision, Methodology, Formal analysis, Conceptualization. **Sara Groppo:** Methodology, Investigation, Data curation, Conceptualization. **Elena Marcello:** Writing – review & editing, Visualization, Validation, Supervision, Methodology, Formal analysis. **Valeria Chiono:** Writing – review & editing, Visualization, Validation, Supervision, Resources, Project administration, Funding acquisition, Formal analysis, Conceptualization.

Funding

ERC-2023-POC EMPATIC has received funding from the European Research Council (ERC) under the European Union's Horizon research and innovation program grant agreement No 101158332. Views and opinions expressed are however those of the author(s) only and do not necessarily reflect those of the European Union or European Research Council Executive Agency (ERCEA). Neither the European Union nor the granting authority can be held responsible for them.

Declaration of competing interest

The authors declare that they have no known competing financial interests or personal relationships that could have appeared to influence the work reported in this paper.

Appendix A. Supplementary data

Supplementary data to this article can be found online at <https://doi.org/10.1016/j.mtbio.2025.102121>.

Data availability

Data will be made available on request.

References

- [1] C. Paoletti, E. Marcello, M.L. Melis, C. Divieto, D. Nurzynska, V. Chiono, Cardiac tissue-like 3D microenvironment enhances route towards human fibroblast direct reprogramming into induced cardiomyocytes by microRNAs, *Cells* 11 (2022) 800, <https://doi.org/10.3390/CELLS11050800>. Page 800 11 (2022).
- [2] B.L. Leonard, B.H. Smail, I.J. LeGrice, Structural remodeling and mechanical function in heart failure, *Microsc. Microanal.* 18 (2012) 50–67, <https://doi.org/10.1017/S1431927611012438>.
- [3] M. Solazzo, F.J. O'Brien, V. Nicolosi, M.G. Monaghan, The rationale and emergence of electroconductive biomaterial scaffolds in cardiac tissue engineering, *APL Bioeng.* 3 (2019), <https://doi.org/10.1063/1.5116579>.
- [4] S. Cho, D.E. Discher, K.W. Leong, G. Vunjak-Novakovic, J.C. Wu, Challenges and opportunities for the next generation of cardiovascular tissue engineering, *Nat. Methods* 19 (2022) 1064–1071, <https://doi.org/10.1038/s41592-022-01591-3>.
- [5] D. Nordsletten, A. Capilnasiu, W. Zhang, A. Wittgenstein, M. Hadjicharalambous, G. Sommer, R. Sinkus, G.A. Holzapfel, A viscoelastic model for human myocardium, *Acta Biomater.* 135 (2021) 441–457, <https://doi.org/10.1016/j.actbio.2021.08.036>.
- [6] X. Lin, Y. Liu, A. Bai, H. Cai, Y. Bai, W. Jiang, H. Yang, X. Wang, L. Yang, N. Sun, H. Gao, A viscoelastic adhesive epicardial patch for treating myocardial infarction, *Nat. Biomed. Eng.* 3 (2019) 632–643, <https://doi.org/10.1038/s41551-019-0380-9>.
- [7] S. Baghersad, A. Sathish Kumar, M.J. Kipper, K. Popat, Z. Wang, Recent advances in tissue-engineered cardiac scaffolds—the progress and gap in mimicking native myocardium mechanical behaviors, *J. Funct. Biomater.* 14 (2023) 269, <https://doi.org/10.3390/JFB14050269>. Page 269 14 (2023).
- [8] O. Chaudhuri, J. Cooper-White, P.A. Janmey, D.J. Mooney, V.B. Shenoy, Effects of extracellular matrix viscoelasticity on cellular behaviour, *Nature* 584 (2020) 535–546, <https://doi.org/10.1038/s41586-020-2612-2>.
- [9] O. Chaudhuri, Viscoelastic hydrogels for 3D cell culture, *Biomater. Sci.* 5 (2017) 1480–1490, <https://doi.org/10.1039/c7bm00261k>.
- [10] O. Chaudhuri, L. Gu, M. Darnell, D. Klumpers, S.A. Bencherif, J.C. Weaver, N. Huebsch, D.J. Mooney, Substrate stress relaxation regulates cell spreading, *Nat. Commun.* 6 (2015) 1–7, <https://doi.org/10.1038/ncomms7365>.
- [11] O. Chaudhuri, L. Gu, D. Klumpers, M. Darnell, S.A. Bencherif, J.C. Weaver, N. Huebsch, H.P. Lee, E. Lippens, G.N. Duda, D.J. Mooney, Hydrogels with tunable stress relaxation regulate stem cell fate and activity, *Nat. Mater.* 15 (2016) 326–334, <https://doi.org/10.1038/nmat4489>.
- [12] M.H. Ghanian, H. Mirzadeh, H. Baharvand, In Situ forming, cytocompatible, and self-recoverable Tough hydrogels based on dual ionic and click cross-linked alginate, *Biomacromolecules* 19 (2018) 1646–1662, <https://doi.org/10.1021/acs.biomac.8b00140>.
- [13] A.E.G. Baker, R.Y. Tam, M.S. Shoichet, Independently tuning the biochemical and mechanical properties of 3D hyaluronan-based hydrogels with oxime and diels-alder chemistry to culture Breast cancer Spheroids, *Biomacromolecules* 18 (2017) 4373–4384, <https://doi.org/10.1021/acs.biomac.7b01422>.
- [14] Z. Emami, M. Ehsani, M. Zandi, H. Daemi, M.-H. Ghanian, R. Foudazi, Modified hydroxyapatite nanoparticles reinforced nanocomposite hydrogels based on gelatin/oxidized alginate via Schiff base reaction, *Carbohydr. Polym. Technol. Appl.* 2 (2021) 100056, <https://doi.org/10.1016/j.carpta.2021.100056>.
- [15] I.A. Marozas, K.S. Anseth, J.J. Cooper-White, Adaptable boronate ester hydrogels with tunable viscoelastic spectra to probe timescale dependent mechanotransduction, *Biomaterials* 223 (2019) 119430, <https://doi.org/10.1016/j.biomaterials.2019.119430>.
- [16] T.E. Brown, B.J. Carberry, B.T. Worrell, O.Y. Dudaryeva, M.K. McBride, C. N. Bowman, K.S. Anseth, Photopolymerized dynamic hydrogels with tunable viscoelastic properties through thioether exchange, *Biomaterials* 178 (2018) 496–503, <https://doi.org/10.1016/j.biomaterials.2018.03.060>.
- [17] S. Tang, B.M. Richardson, K.S. Anseth, Dynamic covalent hydrogels as biomaterials to mimic the viscoelasticity of soft tissues, *Prog. Mater. Sci.* 120 (2021) 100738, <https://doi.org/10.1016/j.pmatsci.2020.100738>.
- [18] Y. Tan, J. Song, Independent and synergistic modulations of viscoelasticity and stiffness of dynamically cross-linked cell-encapsulating ClickGels by covalently tethered polymer Brushes, *Biomacromolecules* 22 (2021) 3408–3415, <https://doi.org/10.1021/acs.biomac.1c00477>.
- [19] D. Wu, W. Wang, D. Diaz-Dussan, Y.Y. Peng, Y. Chen, R. Narain, D.G. Hall, In Situ forming, dual-crosslink network, self-healing hydrogel enabled by a bioorthogonal nopolydiol-benzoxaborolate click reaction with a Wide pH range, *Chem. Mater.* (2019), <https://doi.org/10.1021/acs.chemmater.9b00769>.
- [20] M. Shafiq, O. Ali, S.B. Han, D.H. Kim, Mechanobiological strategies to enhance stem cell functionality for regenerative medicine and tissue engineering, *Front. Cell Dev. Biol.* 9 (2021) 747398, <https://doi.org/10.3389/fcell.2021.747398/BIBTEX>.
- [21] A.R. Cameron, J.E. Frith, J.J. Cooper-White, The influence of substrate creep on mesenchymal stem cell behaviour and phenotype, *Biomaterials* 32 (2011) 5979–5993, <https://doi.org/10.1016/j.biomaterials.2011.04.003>.
- [22] D. Huang, Y. Huang, Y. Xiao, X. Yang, H. Lin, G. Feng, X. Zhu, X. Zhang, Viscoelasticity in natural tissues and engineered scaffolds for tissue reconstruction, *Acta Biomater.* 97 (2019) 74–92, <https://doi.org/10.1016/j.actbio.2019.08.013>.
- [23] D.D. McKinnon, D.W. Domaille, J.N. Cha, K.S. Anseth, Biophysically defined and cytocompatible covalently adaptable networks as viscoelastic 3D cell culture systems, *Adv. Mater.* 26 (2014) 865–872, <https://doi.org/10.1002/adma.201303680>.
- [24] B. Bhana, R.K. Iyer, W.L.K. Chen, R. Zhao, K.L. Sider, M. Likhitanpanichkul, C. A. Simmons, M. Radisic, Influence of substrate stiffness on the phenotype of heart cells, *Biotechnol. Bioeng.* (2010), <https://doi.org/10.1002/bit.22647> n/a-n/a.
- [25] G. Garoffolo, M. Casaburo, F. Amadeo, M. Salvi, G. Bernava, L. Piacentini, I. Chimenti, G. Zaccagnini, G. Milcovich, E. Zuccolo, M. Agrifoglio, S. Ragazzini, O. Baasansuren, C. Cozzolino, M. Chiesa, S. Ferrari, D. Carbonaro, R. Santoro, M. Manzoni, L. Casalis, A. Raucchi, F. Molinari, L. Menicanti, F. Pagano, T. Ohashi, F. Martelli, D. Massai, G.I. Colombo, E. Messina, U. Morbiducci, M. Pesce, Reduction of cardiac Fibrosis by interference with YAP-dependent transactivation, *Circ. Res.* 131 (2022) 239–257, <https://doi.org/10.1161/CIRCRESAHA.121.319373>.
- [26] T. Shi, P. Wang, Y. Ren, W. Zhang, J. Ma, S. Li, X. Tan, B. Chi, Conductive hydrogel patches with high elasticity and Fatigue resistance for cardiac microenvironment remodeling, *ACS Appl. Mater. Interfaces* (2023), <https://doi.org/10.1021/ACSAMI.2C22673>.
- [27] C.M. Madl, L.M. Katz, S.C. Heilshorn, Bio-orthogonally crosslinked, engineered protein hydrogels with tunable Mechanics and Biochemistry for cell encapsulation,

- Adv. Funct. Mater. 26 (2016) 3612–3620, <https://doi.org/10.1002/adfm.201505329>.
- [28] F. Chen, P. Le, G.M. Fernandes-Cunha, S.C. Heilshorn, D. Myung, Bio-orthogonally crosslinked hyaluronate-collagen hydrogel for stroke-free corneal defect repair, *Biomaterials* 255 (2020) 120176, <https://doi.org/10.1016/j.biomaterials.2020.120176>.
- [29] A. Famili, K. Rajagopal, Bio-orthogonal cross-linking chemistry Enables in Situ protein encapsulation and provides sustained release from hyaluronic acid based hydrogels, *Mol. Pharm.* 14 (2017) 1961–1968, <https://doi.org/10.1021/acs.molpharmaceut.7b00067>.
- [30] E. Jain, S. Neal, H. Graf, X. Tan, R. Balasubramaniam, N. Huebsch, Copper-free azide-alkyne cycloaddition for peptide modification of alginate hydrogels, *ACS Appl. Bio Mater.* 4 (2021) 1229–1237, <https://doi.org/10.1021/acsbam.0c00976>.
- [31] H.Y. Yoon, D. Lee, D.K. Lim, H. Koo, K. Kim, Copper-free click chemistry: applications in Drug delivery, cell tracking, and tissue engineering, *Adv. Mater.* 34 (2022), <https://doi.org/10.1002/adma.202107192>.
- [32] G.P. Stola, C. Paoletti, L. Nicoletti, G. Paul, C. Cassino, L. Marchese, V. Chiono, E. Marcello, Internally-crosslinked alginate dialdehyde/alginate/gelatin-based hydrogels as bioinks for prospective cardiac tissue engineering applications, *Int. J. Bioprint* 10 (2024) 544–566, <https://doi.org/10.36922/ijb.4014>.
- [33] S.T. Koshy, R.M. Desai, P. Joly, J. Li, R.K. Bagrodia, S.A. Lewin, N.S. Joshi, D. J. Mooney, Click-crosslinked injectable gelatin hydrogels, *Adv. Healthcare Mater.* 5 (2016) 541–547, <https://doi.org/10.1002/adhm.201500757>.
- [34] M.G. Neira-Velázquez, M.T. Rodríguez-Hernández, E. Hernández-Hernández, A.R. Y. Ruiz-Martínez, Polymer molecular weight measurement, in: *Handbook of Polymer Synthesis, Characterization, and Processing*, John Wiley and Sons, 2013, pp. 355–366, <https://doi.org/10.1002/9781118480793.ch17>.
- [35] O. Smidsrød, Solution properties of alginate, *Carbohydr. Res.* 13 (1970) 359–372, [https://doi.org/10.1016/S0008-6215\(00\)80593-5](https://doi.org/10.1016/S0008-6215(00)80593-5).
- [36] A. Martinsen, G. Skjåk-Bræk, O. Smidsrød, F. Zanetti, S. Paoletti, Comparison of different methods for determination of molecular weight and molecular weight distribution of alginates, *Carbohydr. Polym.* 15 (1991) 171–193, [https://doi.org/10.1016/0144-8617\(91\)90031-7](https://doi.org/10.1016/0144-8617(91)90031-7).
- [37] K.I. Draget, G. Skjåk Bræk, O. Smidsrød, Alginic acid gels: the effect of alginate chemical composition and molecular weight, *Carbohydr. Polym.* 25 (1994) 31–38, [https://doi.org/10.1016/0144-8617\(94\)90159-7](https://doi.org/10.1016/0144-8617(94)90159-7).
- [38] D. Kolotova, L. Petrova, Technology and physico-chemical properties of gelatin from atlantic cod skin, *KnE Life Sci.* 2020 (2020) 426–436, <https://doi.org/10.18502/kds.v5i1.6101>.
- [39] M.A. Masuelli, Mark-houwink Parameters for aqueous-soluble polymers and Biopolymers at various temperatures, *J. Polym. Biopolym. Phys. Chem.* 2 (2014) 37–43, <https://doi.org/10.12691/jpbpc-2-2-2>.
- [40] C.T. Moody, S. Palvai, Y. Brudno, Click cross-linking improves retention and targeting of refillable alginate depots, *Acta Biomater.* 112 (2020) 112–121, <https://doi.org/10.1016/j.actbio.2020.05.033>.
- [41] S.R. Derkach, Y.A. Kuchina, A.V. Baryshnikov, D.S. Kolotova, N.G. Voron'ko, Tailoring cod gelatin structure and physical properties with acid and alkaline extraction, *Polymers* 11 (2019) 1–17, <https://doi.org/10.3390/polym11101724>.
- [42] C. Yu, Z. Yue, M. Shi, L. Jiang, S. Chen, M. Yao, Q. Yu, X. Wu, H. Zhang, F. Yao, C. Wang, H. Sun, J. Li, An intrapericardial injectable hydrogel patch for mechanical-electrical coupling with infarcted myocardium, *ACS Nano* (2022), <https://doi.org/10.1021/acsnano.2c05168>.
- [43] P.K. Smith, R.I. Krohn, G.T. Hermanson, A.K. Mallia, F.H. Gartner, M. D. Provenzano, E.K. Fujimoto, N.M. Goeke, B.J. Olson, D.C. Klenk, Measurement of protein using bicinchoninic acid, *Anal. Biochem.* 150 (1985) 76–85, [https://doi.org/10.1016/0003-2697\(85\)90442-7](https://doi.org/10.1016/0003-2697(85)90442-7).
- [44] S. Kurotsu, T. Sadahiro, R. Fujita, H. Tani, H. Yamakawa, F. Tamura, M. Isomi, H. Kojima, Y. Yamada, Y. Abe, Y. Murakata, T. Akiyama, N. Muraoka, I. Harada, T. Suzuki, K. Fukuda, M. Ieda, Soft matrix promotes cardiac reprogramming via inhibition of YAP/TAZ and suppression of fibroblast Signatures, *Stem Cell Rep.* 15 (2020) 612–628, <https://doi.org/10.1016/j.stemcr.2020.07.022>.
- [45] E. Maksuti, M. Carlsson, H. Arheden, S.J. Kovács, M. Broomé, M. Ugander, Hydraulic forces contribute to left ventricular diastolic filling, *Sci. Rep.* 7 (1) (2017) 1–10, <https://doi.org/10.1038/srep43505>, 7 (2017).
- [46] J.C. Deddens, A.H. Sadeghi, J. Hjortnaes, L.W. van Laake, M. Buijsrogge, P. A. Doevendans, A. Khademhosseini, J.P.G. Sluijter, Modeling the human scarred heart in vitro: toward new tissue engineered models, *Adv. Healthcare Mater.* 6 (2017) 1600571, <https://doi.org/10.1002/adhm.201600571>.
- [47] B.J. Carberry, V.V. Rao, K.S. Anseth, Phototunable viscoelasticity in hydrogels through thioester exchange, *Ann. Biomed. Eng.* 48 (2020) 2053–2063, <https://doi.org/10.1007/s10439-020-02460-w>.
- [48] M.R. Arkenberg, H.D. Nguyen, C.C. Lin, Recent advances in bio-orthogonal and dynamic crosslinking of biomimetic hydrogels, *J. Mater. Chem. B* 8 (2020) 7835–7855, <https://doi.org/10.1039/d0tb01429j>.
- [49] J.S. Choy, S. Leng, G. Acevedo-Bolton, S. Shaul, L. Fu, X. Guo, L. Zhong, J. M. Guccione, G.S. Kassab, Efficacy of intramyocardial injection of Algisyl-LVR for the treatment of ischemic heart failure in swine, *Int. J. Cardiol.* 255 (2018) 129–135, <https://doi.org/10.1016/j.ijcard.2017.09.179>.
- [50] E. Ruvinov, S. Cohen, Alginate biomaterial for the treatment of myocardial infarction: Progress, translational strategies, and clinical outlook, *Adv. Drug Deliv. Rev.* 96 (2016) 54–76, <https://doi.org/10.1016/j.addr.2015.04.021>.
- [51] R.J. Lee, A. Hinson, R. Bauernschmitt, K. Matschke, Q. Fang, D.L. Mann, R. Dowling, N. Schiller, H.N. Sabbah, The feasibility and safety of Algisyl-LVRTM as a method of left ventricular augmentation in patients with dilated cardiomyopathy: initial first in man clinical results, *Int. J. Cardiol.* 199 (2015) 18–24, <https://doi.org/10.1016/j.ijcard.2015.06.111>.
- [52] M.E. Klontzas, H. Drissi, A. Mantalaris, M.E. Klontzas, H. Drissi, A. Mantalaris, The use of alginate hydrogels for the culture of mesenchymal stem cells (MSCs): in vitro and in vivo Paradigms, *Alginates Recent Uses Nat. Polym.* (2019), <https://doi.org/10.5772/intechopen.88020>.
- [53] B. Sarker, R. Singh, R. Silva, J.A. Roether, J. Kaschta, R. Detsch, D.W. Schubert, I. Cicha, A.R. Boccaccini, Evaluation of fibroblasts adhesion and proliferation on alginate-gelatin crosslinked hydrogel, *PLoS One* 9 (2014) e107952, <https://doi.org/10.1371/JOURNAL.PONE.0107952>.
- [54] Y. Deng, A. Shavandi, O.V. Okoro, L. Nie, Alginate modification via click chemistry for biomedical applications, *Carbohydr. Polym.* 270 (2021) 118360, <https://doi.org/10.1016/j.carbpol.2021.118360>.
- [55] C.T. Moody, A.E. Brown, N.P. Massaro, A.S. Patel, P.A. Agarwalla, A.M. Simpson, A.C. Brown, H. Zheng, J.G. Pierce, Y. Brudno, Restoring Carboxylates on highly modified alginates improves gelation, tissue retention and systemic capture, *Acta Biomater.* 138 (2022) 208–217, <https://doi.org/10.1016/j.actbio.2021.10.046>.
- [56] V.X. Truong, K.M. Tsang, G.P. Simon, R.L. Boyd, R.A. Evans, H. Thissen, J. S. Forsythe, Photodegradable gelatin-based hydrogels prepared by bioorthogonal click chemistry for cell encapsulation and release, *Biomacromolecules* 16 (2015) 2246–2253, <https://doi.org/10.1021/acs.biomac.5b00706>.
- [57] J. Kim, Y.-J. Choi, C.-W. Gal, A. Sung, H. Park, H.-S. Yun, Development of an alginate-gelatin bioink enhancing osteogenic differentiation by gelatin release, *Int. J. Bioprint* 9 (2023) 660, <https://doi.org/10.18063/ijb.v9i2.660>.
- [58] B. Stubbe, A. Mignon, H. Declercq, S. Van Vlierbergh, P. Dubrue, Development of gelatin-alginate hydrogels for Burn Wound treatment, *Macromol. Biosci.* 19 (2019), <https://doi.org/10.1002/mabi.201900123>.
- [59] N. Lagneau, P. Tournier, B. Halgand, F. Loll, Y. Maugars, J. Guicheux, C. Le Visage, V. Delplace, Click and bioorthogonal hyaluronic acid hydrogels as an ultra-tunable platform for the investigation of cell-material interactions, *Bioact. Mater.* 24 (2023) 438–449, <https://doi.org/10.1016/j.bioactmat.2022.12.022>.
- [60] A. Diana, G.I. Truglio, E. Petricci, D. Lanari, Expanding the bioorthogonal chemistry toolbox: innovative synthetic strategies for cyclooctynes, *Org. Biomol. Chem.* 23 (2025) 5441–5456, <https://doi.org/10.1039/d5ob00456j>.
- [61] S. Bernard, R.A. Kumar, K. Porte, P. Thuéry, F. Taran, D. Audisio, A practical synthesis of valuable strained eight-membered-ring Derivatives for click chemistry, *Eur. J. Org. Chem.* (2018) 2000–2008, <https://doi.org/10.1002/ejoc.201800139> (2018).
- [62] G. Ruocco, A. Zoso, L. Mortati, I. Carmagnola, V. Chiono, Biomimetic Electrospun scaffold-based in vitro model resembling the Hallmarks of human myocardial fibrotic tissue, *ACS Biomater. Sci. Eng.* 9 (2023) 4368–4380, <https://doi.org/10.1021/acsbiomaterials.3c00483>.
- [63] M. Pesce, G.N. Duda, G. Forte, H. Girao, A. Raya, P. Roca-Cusachs, J.P.G. Sluijter, C. Tschöpe, S. Van Linthout, Cardiac fibroblasts and mechanosensing in heart development, health and disease, *Nat. Rev. Cardiol.* 20 (2023) 309–324, <https://doi.org/10.1038/s41569-022-00799-2>.
- [64] H. Zhan, S. Jiang, A.M. Jonker, I.A.B. Pijpers, D.W.P.M. Löwik, Self-recovering dual cross-linked hydrogels based on bioorthogonal click chemistry and ionic interactions, *J. Mater. Chem. B* 8 (2020) 5912–5920, <https://doi.org/10.1039/d0tb01042a>.
- [65] G.F. Sousa, S. Afewerki, D. Dittz, F.E.P. Santos, D.O. Gontijo, S.R.A. Scalzo, A.L. C. Santos, L.C. Guimaraes, E.M. Pereira, L.S. Barcelos, S.J.H. Do Monte, P.P. G. Guimaraes, F.R. Marciano, A.O. Lobo, Catalytic-free click chemistry for engineering Chondroitin sulfate-multiarmed PEG hydrogels for skin tissue engineering, *J. Funct. Biomater.* 13 (2022) 1–16, <https://doi.org/10.3390/jfb13020045>.
- [66] D. Testore, A. Zoso, G. Kortaberria, M. Sangermano, V. Chiono, Electroconductive photo-curable PEGDA-gelatin/PEDOT:PSS hydrogels for prospective cardiac tissue engineering application, *Front. Bioeng. Biotechnol.* 10 (2022), <https://doi.org/10.3389/fbioe.2022.897575>.
- [67] Z. Wu, Z. Yang, D. Sha, Y. Ma, B.Y.S. Kim, W. Jiang, Y. Yuan, C. Liu, Injectable, viscoelastic hydrogel precisely regulates developmental tissue regeneration, *Chem. Eng. J.* 434 (2022) 133860, <https://doi.org/10.1016/j.cej.2021.133860>.
- [68] Y. Ma, T. Han, Q. Yang, J. Wang, B. Feng, Y. Jia, Z. Wei, F. Xu, Viscoelastic cell microenvironment: hydrogel-based Strategy for recapitulating dynamic ECM mechanics, *Adv. Funct. Mater.* 31 (2021), <https://doi.org/10.1002/adfm.202100848>.
- [69] J. Lou, R. Stowers, S. Nam, Y. Xia, O. Chaudhuri, Stress relaxing hyaluronic acid-collagen hydrogels promote cell spreading, fiber remodeling, and focal adhesion formation in 3D cell culture, *Biomaterials* 154 (2018) 213–222, <https://doi.org/10.1016/j.biomaterials.2017.11.004>.
- [70] K.H. Vining, A. Stafford, D.J. Mooney, Sequential modes of crosslinking tune viscoelasticity of cell-instructive hydrogels, *Biomaterials* 188 (2019) 187–197, <https://doi.org/10.1016/j.biomaterials.2018.10.013>.
- [71] G.P. Stola, C. Paoletti, L. Nicoletti, G. Paul, C. Cassino, L. Marchese, V. Chiono, E. Marcello, Internally-crosslinked alginate dialdehyde/alginate/gelatin-based hydrogels as bioink for prospective cardiac tissue engineering applications, *Int. J. Bioprint* (2024) 4014, <https://doi.org/10.36922/ijb.4014>.
- [72] A. Lueckgen, D.S. Garske, A. Ellinghaus, R.M. Desai, A.G. Stafford, D.J. Mooney, G. N. Duda, A. Cipitria, Hydrolytically-degradable click-crosslinked alginate hydrogels, *Biomaterials* 181 (2018) 189–198, <https://doi.org/10.1016/j.biomaterials.2018.07.031>.
- [73] Y. Tan, H. Huang, D.C. Ayers, J. Song, Modulating viscoelasticity, stiffness, and degradation of synthetic cellular Niches via stoichiometric tuning of covalent versus dynamic noncovalent cross-linking, *ACS Cent. Sci.* 4 (2018) 971–981, <https://doi.org/10.1021/acscentsci.8b00170>.
- [74] J. Lang, Y. Li, Z. Ye, Y. Yang, F. Xu, G. Huang, J. Zhang, F. Li, Investigating the effect of substrate stiffness on the redox state of cardiac fibroblasts using scanning

- electrochemical microscopy, *Anal. Chem.* 93 (2021) 5797–5804, https://doi.org/10.1021/ACS.ANALCHEM.0C05284/SUPPL_FILE/AC0C05284_SI_001.PDF.
- [75] M. Galdyszyńska, P. Radwańska, J. Szymański, J. Drobnik, The stiffness of cardiac fibroblast substrates Exerts a regulatory influence on collagen metabolism via $\alpha\beta1$ Integrin, FAK and Src Kinases, *Cells* 10 (2021) 3506, <https://doi.org/10.3390/CELLS10123506>. Page 3506 10 (2021).
- [76] S. Nam, Y.H. Lin, T. Kim, O. Chaudhuri, Cellular pushing forces during Mitosis drive mitotic elongation in collagen gels, *Adv. Sci.* 8 (2021) 2000403, <https://doi.org/10.1002/ADVS.202000403>.
- [77] J. Zheng, R. Sun, H. Chen, T. Zeng, T. Yoshitomi, N. Kawazoe, Y. Yang, G. Chen, Morphological dependence of Breast cancer cell responses to Doxorubicin on micropatterned surfaces, *Polymers* 14 (2022) 2761, <https://doi.org/10.3390/POLYM14142761>. Page 2761 14 (2022).
- [78] A. Elosegui-Artola, A. Gupta, A.J. Najibi, B.R. Seo, R. Garry, C.M. Tringides, I. de Lázaro, M. Darnell, W. Gu, Q. Zhou, D.A. Weitz, L. Mahadevan, D.J. Mooney, Matrix viscoelasticity controls spatiotemporal tissue organization, *Nat. Mater.* 22 (2023) 117–127, <https://doi.org/10.1038/s41563-022-01400-4>.
- [79] M. Jury, I. Matthiesen, F. Rasti Borojeni, S.L. Ludwig, L. Civitelli, T.E. Winkler, R. Selegård, A. Herland, D. Aili, Bioorthogonally cross-linked hyaluronan–laminin hydrogels for 3D neuronal cell culture and biofabrication, *Adv. Healthcare Mater.* 11 (2022) 2102097, <https://doi.org/10.1002/adhm.202102097>.